



Identification of seasonal variation of water turbidity using NDTI method in Panchet Hill Dam, India

Sumanta Bid¹ · Giyasuddin Siddique¹

Received: 21 January 2019 / Accepted: 10 May 2019 / Published online: 22 May 2019
© Springer Nature Switzerland AG 2019

Abstract

Sedimentation in reservoir is a common problem in any multipurpose river valley project and is effective upon the performance of it. Every dam has an estimated volume of water holding capacity at the time of inception, but it gradually reduces by siltation. The presence of sediments in water causes turbidity and it slowly precipitates on the floor of the reservoir. Normalized difference turbidity index (NDTI) is a remote sensing technique widely used to identify the water turbidity, which is the ratio of red and green bands of solar spectrum. In Panchet Dam actual rate of siltation exceeds the assumed rate that fills up the entire reservoir area at a faster rate. In this situation, the study has been conducted to explain the variation of water turbidity of the dam throughout the year 2015. Major findings of the study indicate that the turbidity level jumps from 60 NTU to 700 NTU in the monsoon. High turbid water covers 50.57%, 64.22% and 52.79% area of the reservoir in July, August and September, respectively. In contrast, coverage of low turbid water is more than 71.68% in the months of February and June. The medium turbid water covers less than 35.82% area throughout the year except the months of September and October. High level of correlation exists ($R^2=0.900$) between NDTI values and total suspended sediments concentration in mg/L ($N=15$, $p<0.05$) with minimal RMSE (13.59). Variation of seasonal turbidity and different types of turbidity are significant at 95% ($p<0.05$) level of significance. The paper is an attempt to probe into the seasonal variation of water turbidity of the dam with the application of NDTI method and related statistical measures.

Keywords Panchet Hill Dam · Sedimentation · NDTI · Water turbidity · TSS

Introduction

Catchment areas eroded by headwater are known to be prime contributors of sediments delivered to the rivers of larger lowland systems (Meybeck et al. 2003; Mano et al. 2009). The silting phenomenon gradually reduces the expected lifespan of a reservoir by the shrinkage of water storage capacity and it directly affects the performance of the dam (Morris and Fan 1998; Jain and Singh 2003; Grade 2006; Issa et al. 2017). Most common and optically sensitive water constituent, namely, turbidity has usually been estimated using remote sensing data (Aguirre-Gomez 2000; Kratzer et al. 2000; Doxaran et al. 2002; Tyler et al. 2006; Teodoro

et al. 2008; Olmanson et al. 2013; Papoutsas et al. 2014, Garg et al. 2017). Normalized difference turbidity index (NDTI) method has been adapted to retrieve turbidity using multi-spectral remote sensing data.

Suspended sediment is the main component material affecting surface water quality (Chalov et al. 2017a; Trinh et al. 2018). Highly turbid water body is an important effective factor for any dam as it obstructs beneficial aspects of a multipurpose damming project (He et al. 1994). Quick and effective monitoring of water quality of a dam in order to sustain a healthy supply system of drinking water and industrial-agricultural water usage are very difficult (Chen et al. 2009). Water turbidity monitoring of rivers was based traditionally on fixed stations by collecting water samples and then analyzing in laboratory. This method was tedious, time consuming and costly, but the problem could be overcome by the use of remotely sensed satellite images that potentially offer wide area coverage, as well as long-term and continuous water turbidity measurements and monitoring of sedimentation (Molo et al. 1989; Collins and Walling

✉ Sumanta Bid
sumantabid460@gmail.com

Giyasuddin Siddique
gsbu2008@gmail.com

¹ Department of Geography, The University of Burdwan,
Golapbag, Purba Bardhaman, West Bengal 713104, India

2004; Martínez-Carreras et al. 2010). The field works of Chen et al. (2009), Ghosh and Islam (2016), Guchhait et al. (2016), Chalov et al. (2017a, b), Moeeni et al. (2017), Moeeni and Bonakdari (2017), Zaji et al. (2018), Trinh et al. (2018), Bonakdari et al. (2019) and Zaji et al. (2019) provide larger scopes of remote sensing application both in theoretically and practically for transport, deposition and monitoring of sediments that are published recently in esteemed journals. In this paper the water turbidity has been estimated by NDTI method and classified into three categories, viz. low, medium and high on the basis of mean and standard deviation of resulted NDTI value using satellite images provided by the USGS, with the help of Arc GIS software, version 10.3. It calculates the area of variable concentration of turbidity in 12 individual months of the year 2015, dividing into three broad categories. The data related to the different types of turbid coverage of the dam has been collected from the 12 NDTI maps of the mentioned year and has been categorized into four distinct seasons, viz. winter, pre-monsoon, monsoon and post-monsoon to examine the seasonal variation of water turbidity. The information generated in the present study could be used as an important input in the sustainable management of water and its quality. Continuous monitoring and assessment of siltation of the reservoir is vital and significant also to preserve and protect actual structure of the dam. The current study has some utility to monitor and quantify suspended sediment load, compute area under different types of turbidity cover of the reservoir and also has some cost and time benefits than ground truth method to analyze the sediment character.

The study area

Location of the study area

In broader term, the eastern margin of the Chotanagpur plateau, covering the south-eastern border of the Jharkhand State and the western margin of the West Bengal State has been considered as the area under study. In terms of district level administrative units, the study area encompasses the north-eastern portion of Puruliya district. It is bounded by the Neturia and Raghunathpur I and II Blocks of Puruliya district on the east; Saltora and Mejia Blocks of Bankura district on the south; Paschim Bardhaman district on the north-east and Dhanbad district of Jharkhand State on the north and north western part. To the north-east of this area lies the 643.5 m high Panchakot or Panchet Hill which is 5 km long and spreads from north to south as a long round ridge. The dam has been built across the Damodar River, 5 km above the confluence with the Barakar which is the tri-junction of Dhanbad, Bardhaman and Puruliya districts (Gaz.Pur, 1985). Location of the area is shown in Fig. 1.

The Panchet Hill Dam

The Panchet Hill Dam is one of the most important strategic multipurpose river valley projects of India maintained by the authority of the Damodar Valley Corporation (DVC) which is constructed in 1959 by impeding of the river Damodar. It is stretched from $86^{\circ}29'30''\text{E}$ latitude to $86^{\circ}45'21''\text{E}$ latitude and $23^{\circ}36'11''\text{N}$ longitude to $23^{\circ}42'40''\text{N}$ longitude. The major purpose of the dam was to control flood frequency of the Damodar River, fishing, irrigation for cultivation, supply of drinking water and hydroelectric projects. The basic features of the dam are highlighted in Table 1. Rate of siltation in the reservoir is high due to presence of sedimentary rock in the upper catchment area. Reservoirs are classified into four categories based on the shape factor 'M' and the nature, the Panchet reservoir is very close to type II, as 'flood plain-foot hill type' of reservoir (Table 2). Shape factor 'M' represents the reciprocal slope of the straight line that can be calculated from plotting the relationship of water depth at dam site in the Y-axis against the storage capacity in the X-axis on a logarithmic scale (Borland and Miller 1958; Mohammadzadeh-Habili et al. 2009; Mohammadzadeh-Habili and Heidarpour 2010; Kaveh et al. 2013).

Geology

The area is dominated by metamorphic rocks of Proterozoic age and sedimentaries of Gondwana age. Rocks of younger age include only Quaternary sediments mixed with residual soil at places and are confined to narrow drainage basin of the Damodar River (Geological Survey of India 1991). The Panchet Hill in the Raniganj Coalfield area is formed of coarse-grained feldspathic sandstones with thin greenish brown shale and red claystone with a few beds of impure limestone in the upper part and conglomerate with laterite nodules at the base of the *Panchet Formation*. Evidences of the fossil floral assemblage accommodate the Panchet in Early Triassic period (Valdiya 2016). Geological strata of the Panchet Basin and Succession of the *Panchet Formation* are shown in Fig. 2 and Table 3, respectively.

Physiography

The Damodar River runs a distance of 26 km within the area under review. The elevation of its entry part is 175 m but rises up to 100 m in the exit part. Thus the slope in this part is about $10^{\circ}/\text{km}$. Such slope encourages considerable erosion activity which is further enhanced by the bareness and friability of soil from the valley sides and upper parts where vegetal cover is absent. Thus the slope areas experience intense erosion and transportation. The transported

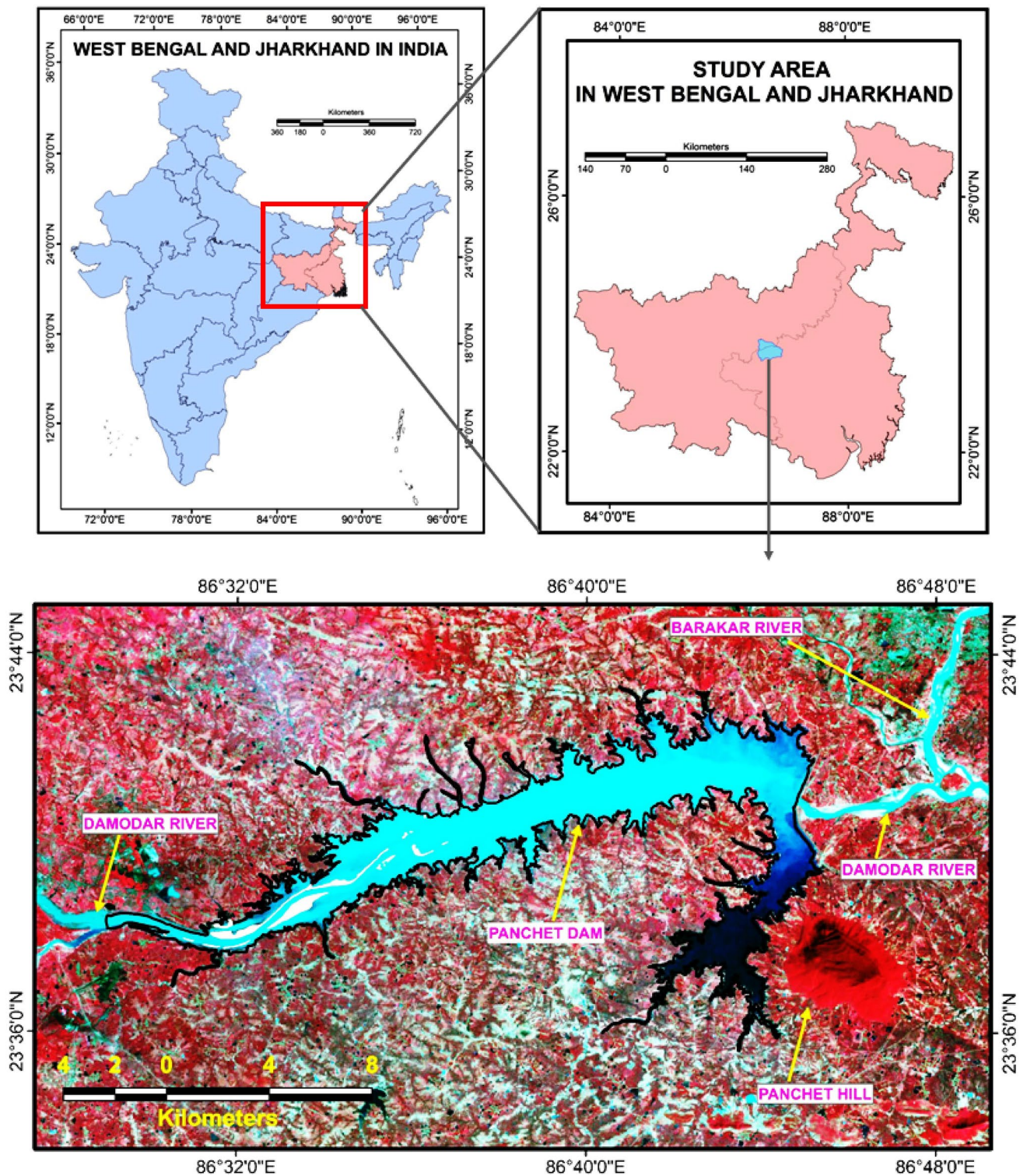


Fig. 1 Location of the Panchet Hill Dam. Source of the used Landsat 8 OLI (Operational Land Imager) data is United States Geological Survey (USGS) and downloaded from the link from www.glovis.usgs.gov

on January 7, 2014 (Image ID-0101503131929_00010) of 139/44 path and row

Table 1 Basic information about the Panchet Hill Dam

Construction started	1952
Year of opening	6/12/1959
Impounds	Damodar river
Types of dam	Earthen dam with concrete spillway
Height	45 m
Width (in base)	10.67 m
Length	6777 m
Surface area	27.92 km ²
Catchment area	10,961 km ²
Average annual basin rainfall	114 cm
Gross storage capacity	1497.54 million m ³
Dead storage capacity	170.37 million m ³
Average annual run-off volume	4540 million m ³
Irrigated land	28 lakh hectares
Power generation capacity	2 × 40 MW

Source: www.dvc.gov.in

Table 2 Reservoir classification according to shape factor 'M' (Borland and Miller 1958)

Types of reservoir	Classification	Shape factor 'M'
I	Lake	3.5–4.5
II	Flood plain–foot hill	2.5–3.5
III	Hill	1.5–2.5
IV	Gorge or normally empty	1.0–1.5

materials are deposited on the bed of the dam thereby modifying the slope character (Siddique and Bid 2017). In Fig. 3 AB, CD, EF, GH, and IJ, there are five cross sections drawn across the dam and the slopes measured are 14°/km, 10°/km, 13°/km, 10°/km and 26°/km, respectively, that indicate a basin like feature of the area. Cross profile of all section lines highlight a syncline and basin shaped topography surrounding the dam and this topography assists to accelerate the soil erosion in the contiguous area of the dam.

Climate and hydrology

The area is characterized by dry and wet sub-humid tropical climate under the regime of south west monsoon. The tract falls in the 'Aw' type of climate (Spate and Farmer 1954) as per Koppen's scheme of climatic classification. Temperature varies from 3.8 °C in winter to 52 °C in summer and annual rainfall varies from 1100 to 1500 mm. Figure 4 displays 10 years average temperature and rainfall graphs from 1971 to 2010 and represents the climatic condition of the decades 1980, 1990, 2000 and 2010. The Damodar being the main river flows from the north-west

to the south-east direction along the area. A number of first-order and second-order streams supply adequate run-off with full of eroded sediment to the dam.

Vegetation cover

In the pre-dam phase, the Panchet basin area was covered by dense vegetation. A number of dense vegetation patches, mainly forests, are identified in the topographical map published in 1927. These types of vegetation patches has been totally removed in the post-dam period, except a residual vegetation patch on the Panchet hill top area and a few degraded vegetation patches exposed on the topographical map of 1976. Rapid loss of vegetation cover encourages soil erosion in a faster rate and consequently suspended sediment load is reciprocally contributed with the surface runoff. A drastic change in vegetation cover and species is noticed in the last two decades. In the previous work Bid (2016) has calculated category-wise vegetation change from 1990 to 2014 with the help of NDVI technique. Statistics of changing vegetation category is shown in Table 4.

Materials and methods

Background of the present work

Siltation is a crucial problem related to all types of dam. Every dam has an estimated life span at the time of its inception, but becomes blocked by siltation that reduces the life span. The assumed rate of siltation for the Panchet Dam was only 6.67 ha m/1000 km² during its inception, but actual siltation has been measured to 10.48 ha m/1000 km² at present. Therefore, an increase of 57% is really worrisome (Singh and Banerji 2002; Siddique and Bid 2017) which fills up the entire dam at a faster rate. The trend line of Fig. 5a indicates present condition of the dam that is almost 30% storage capacity has been reduced within the 60 years of its inception. Figure 5b, c shows the estimation curves of 50% and 100% loss of storage capacity of the reservoir correspondingly. In round figure, the total capacity of the dam was 1600 million m³ at the time of its inception but 50% capacity seems to be lost in the year 2090 and it takes only 130 years. The dam will be totally filled up around the year 2210 that reveals total life span of the dam may be more or less 250 year. In this circumstance, we take an attempt to investigate sedimentation character of the dam. Therefore, we have considered the NDTI technique to investigate the character of turbidity and suspended sediment load of the dam throughout the year 2015 and compared the result to the ground truth values derived from the field investigation data to validate the result obtained from the remotely sensed technique of NDTI.

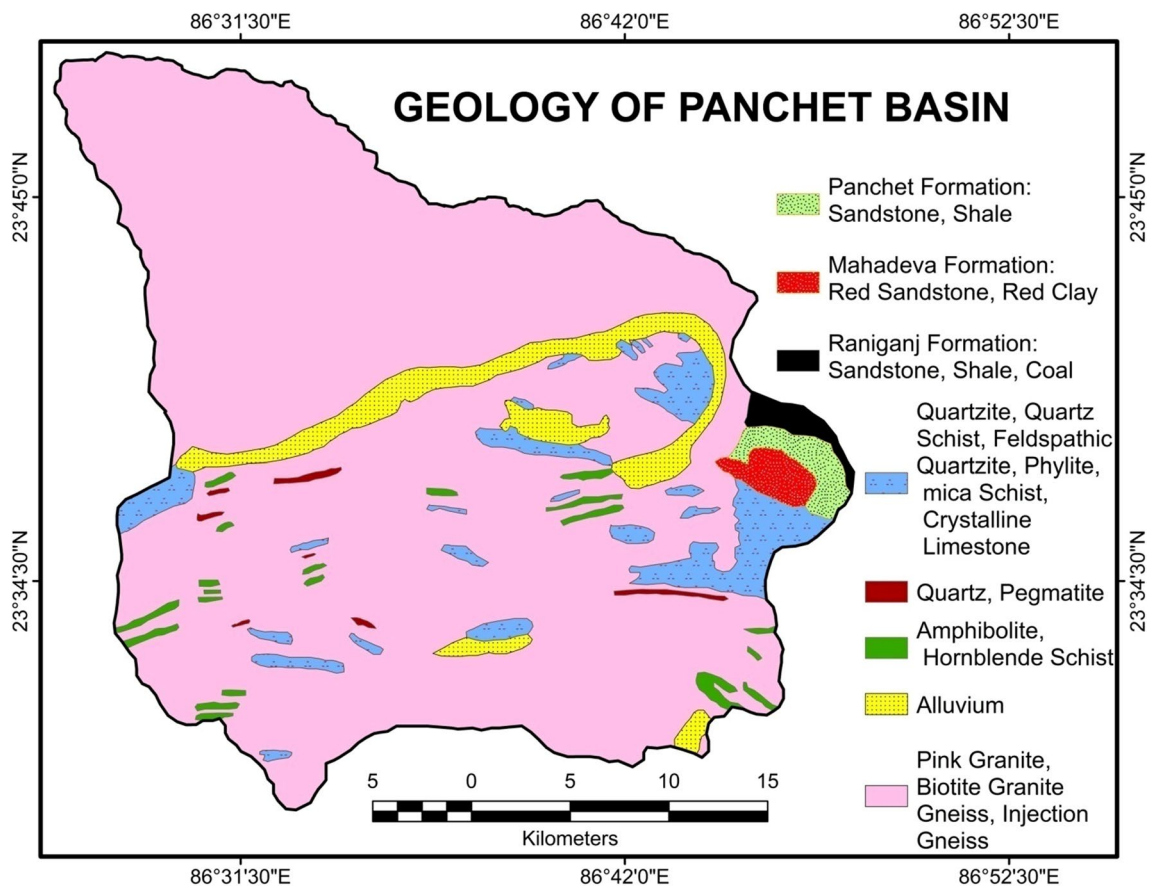


Fig. 2 Geological structure of the Panchet Basin. The map is prepared by authors on the basis of Geological Quadrangle Map—Puruliya Quadrangle (731), Geological Survey of India, Calcutta, Government of India, 1991

Table 3 Geological succession of the Panchet Formation

Age	Formation	Damodar basin
Cretaceous	Lower	Rajmahal
<i>Jurassic</i>		
Upper		
Middle	Jabalpur	Dubrajpur
Lower		
<i>Triassic</i>		
Upper	Mahadev	Mahadeva
Middle	Denwa	
Lower	Panchet	Panchet
<i>Permian</i>		
Upper	Raniganj	Raniganj
Middle	Barren Measures	Kulti
Lower	Barakar	Barakar
	Karharbari	Karharbari
	Talchir	Talchir

Source: Valdiya 2016

Use of remotely sensed data

Landsat 5 TM (Thematic Mapper) and Landsat 8 OLI (Operational Land Imager) satellite data of 30-m resolution are used to construct classified turbidity maps of 2015. On the basis of those maps, areal coverage under different categories of turbidity is calculated. Out of 12 satellite data of 2015 used in the present work, 11 images are LANDSAT 8 OLI type data. We are compelled to use one satellite data of LANDSAT 5 TM for the month of July because of unavailability of clear and cloud-free LANDSAT 8 OLI image of the particular month. Spatial resolution and other features of LANDSAT 5 TM are more or less same with the characters of LANDSAT 8 OLI data; hence the difference of the NDTI result is minimal between the LANDSAT 8 OLI data and LANDSAT 5 TM data. Major features of the used satellite data are given in Table 5. Only red and green bands are extracted from entire data acquired from the snaps of 12 different

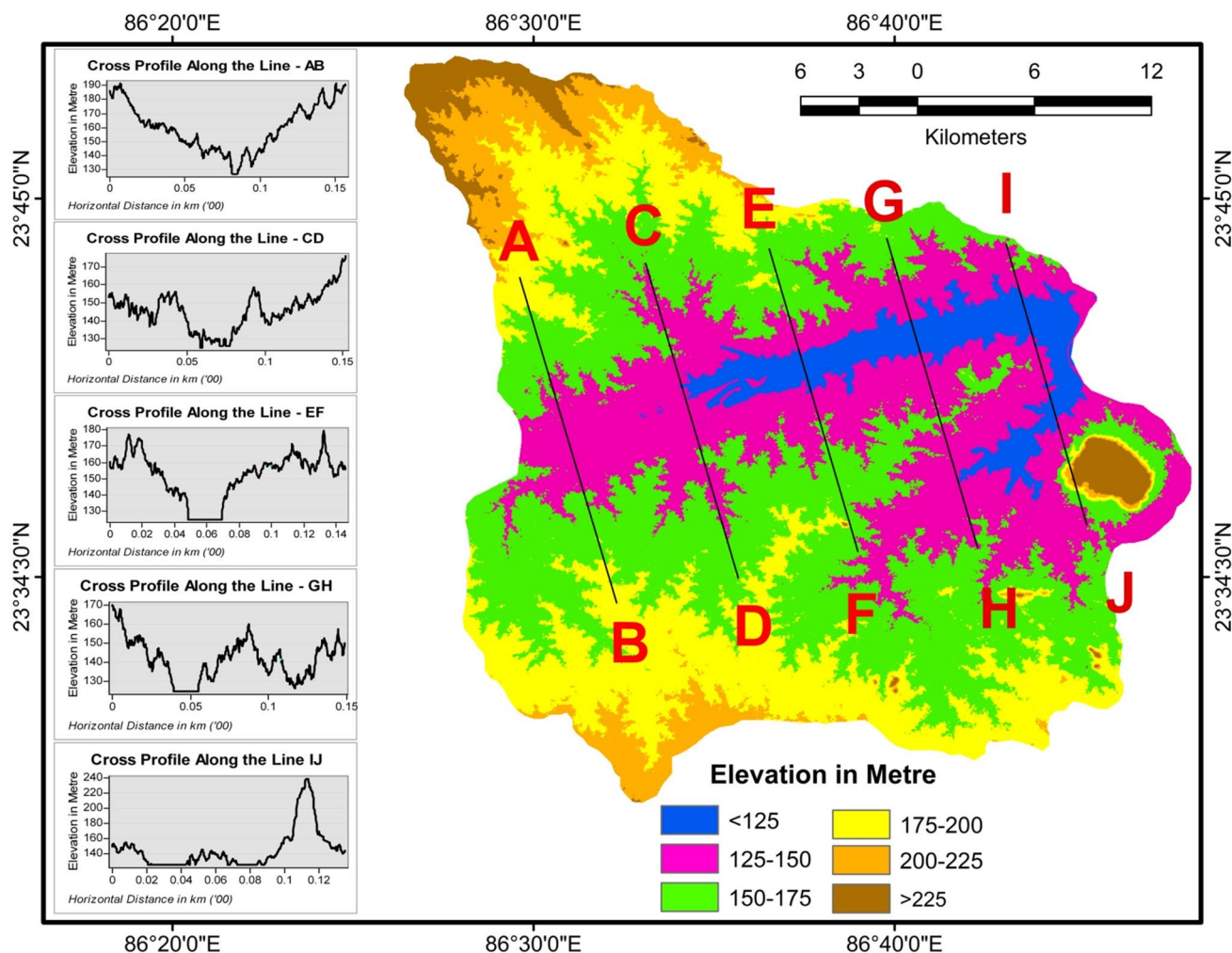


Fig. 3 Cross section and cross profile across the dam. The map is prepared on the basis of ASTER DEM data of 30-m resolution, acquired from the link <http://glcf.umd.edu/data/aster/>

dates to build the individual turbidity maps. In case of LANDSAT-8 OLI data, band 3 and band 4 have been used in the band ratio. Band 3 is green and its wave length is 0.525–0.600 μm while band 4 is red band with wave length of 0.630–0.680 μm . Band 2 and band 3 are used in the case of LANDSAT-5 TM data. Band 2 is green and its wave length is 0.53–0.61 μm whereas band 3 is red and wave length is 0.63–0.69 μm .

A semi-automated approach has been adopted to remove cloud. Satellite data is converted into light reflectance value from digital number by atmospheric and radiometric correction using ERDAS IMAGINE 9.2 software through cloud detection, color balancing and image patching processes that make cloud-free images (Qu et al. 2017; Rahaman et al. 2017; Shaharum et al. 2018). Raw satellite images were converted to specific map projection using geometric correction. The whole work has been done with the help Arc GIS software of version 10.2.1. Reflectance

of different bands and FCC combination of the reservoir water are represented in Fig. 6.

Field survey and sample data

Field investigation was conducted on 27/02/2015, 02/05/2015, 19/08/2015 and 26/11/2015 by selecting a single date from each season at an interval of three months average throughout the year 2015. 15 in situ stations have randomly selected over the Panchet Dam to collect water sample. Sampling points are recorded by the hand held GPS (Global Positioning System). 1-L plastic containers are used to preserve water sample and generate a ground truth data on sediment concentration in milligram per liter volume of water (mg/L) by filtering (filtered by EZ-Park Filters of 0.22 μm) and weighting of sediments in laboratory. 15 samples are collected from field investigations

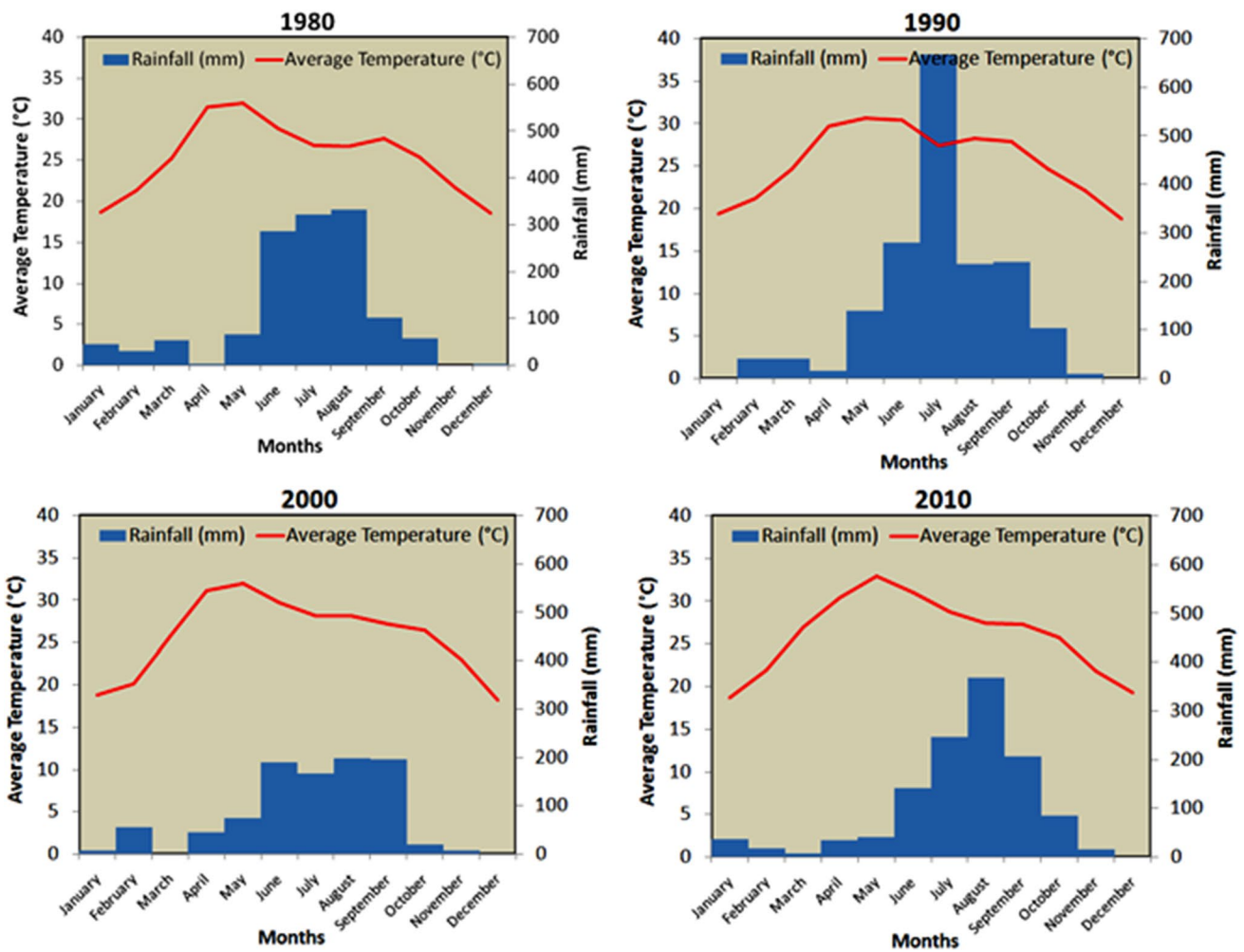


Fig. 4 10-year average climatic condition. Climographs are prepared on the basis of WRIS (Water Resource Information System) data, Government of India

Table 4 Density class-wise change of vegetation cover of the area from 1990 to 2014

NDVI density classes (vegetation cover)	1990 NDVI classes area		2014 NDVI classes area		Change between 1990 and 2014		Average rate of change	
	km ²	%	km ²	%	km ²	%	km ² /year	%
Low (0.2–0.3)	1539.61	89.02	449.24	86.97	–1090.37	–70.82	–45.43	–2.95
Medium (0.3–0.4)	169.23	9.79	48.54	9.40	–120.69	–71.37	–5.02	–2.97
High (> 0.4)	20.57	1.19	18.77	3.63	–1.80	–17.64	–0.08	–0.74
Total	1729.41	100.00	516.55	100.00	–1212.86	–	–	–

Data source: Bid 2016

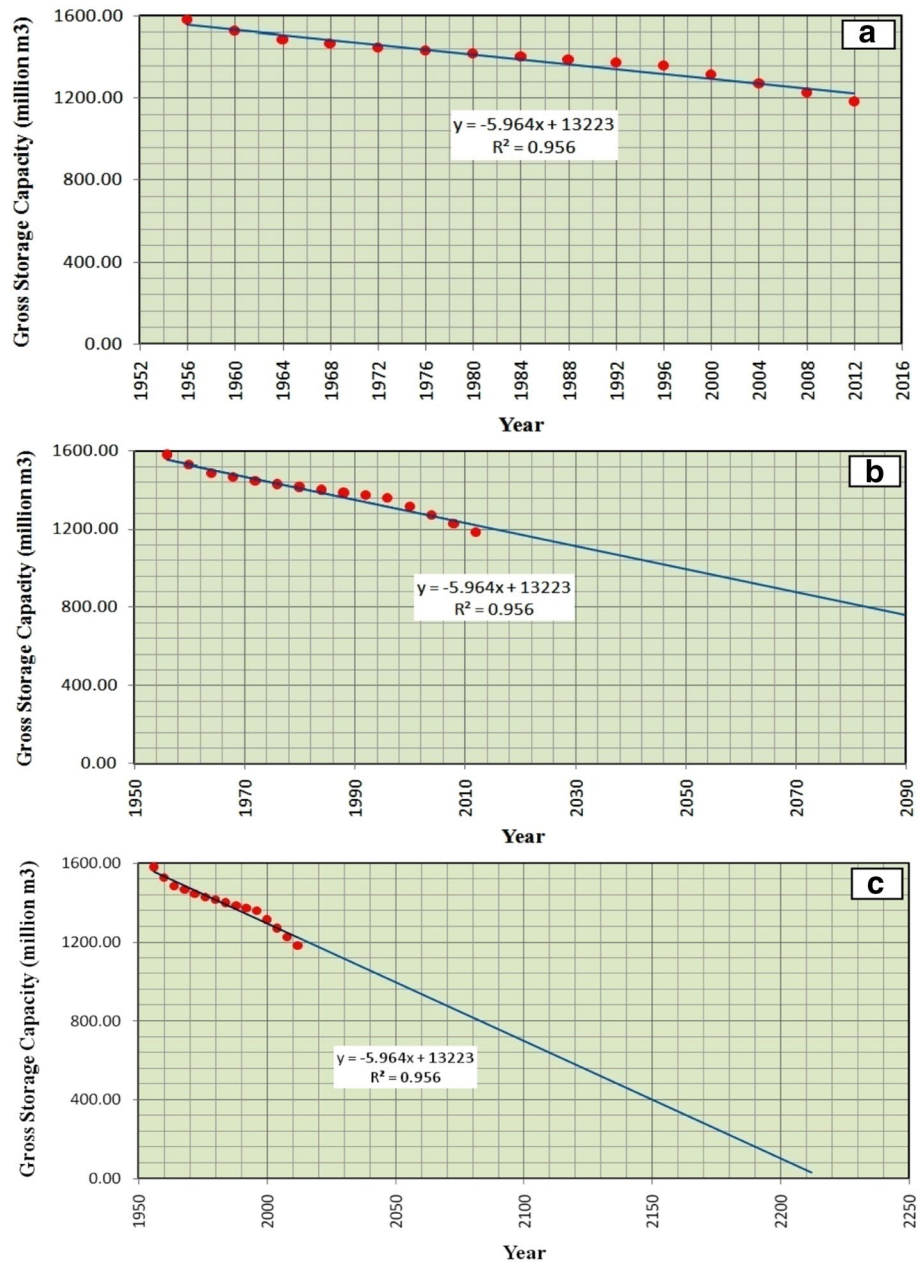
each time and total sample was $n = 60$ (15×4). Sample collection points are shown in Fig. 7.

Normalized difference turbidity index (NDTI)

In the normalized difference turbidity index (NDTI), pure or sediment-free water has a specific radiometric response: its

reflectance is weak in green (less than 10%), becomes very small in red and quasi null in NIR. The increase in turbidity and its associated radiometric responses make the open water features behave like bare soil (Guyot 1989; Lacaux et al. 2007; Gardelle et al. 2010). As turbidity level of water increases due to increase of suspended particles in water, reflectance of the red band is more than that of the green

Fig. 5 Change of gross storage capacity of the Panchet reservoir. **a** Present situation of storage capacity, **b** estimation of 50% storage capacity loss (c). Estimation of 100% storage capacity loss. The diagram is prepared on the basis of CWC (Central Water Commission) data, Government of India, 2013



band (Islam and Sado 2006). This spectral characteristic of the turbid water can be used for the detection of turbid water pixels and has been captured in the NDTI. Since values of the red radiometric responses are much larger than that of the green ones, the relationship between green and red wavelengths is reversed (Verbyla 1995; Campbell 1996). NDTI is the ratio of red and green bands. The band combination formula for determination of the NDTI is:

$$\text{NDTI} = (\text{red band} - \text{green band}) / (\text{red band} + \text{green band}). \quad (1)$$

The technique is used to generate qualitative turbidity levels as low, moderate and high turbid concentration based

on signature statistics, mean and standard deviations of the NDTI values (Townshend and Justice 1986; Tucker and Sellers 1986; Sharma et al. 2014). Generally, NDTI varies from -0.2 to greater than $+0.25$, whereas lower value indicates clear water and higher value is the representative of highly turbid water (Alka et al. 2014).

Turbidity is the cloudiness of water or intervention in way of light due to suspended sediment material. Positive correlation between concentration of suspended sediments and remotely sensed signals is established and total suspended sediments load can be estimated through regression analysis. The relationship of suspended sediment concentration with reflectance depends on many factors such as optical

Table 5 Important features of the used satellite data

Sl no.	Date of acquired	Spacecraft ID/sensor	Data type	Path	Row	sun elevation	Sun azimuth	Projection	Datum	UTM zone	Spatial resolution	Orientation cloud cover (%)
1	10/01/15	LANDSAT-8	OLI	139	44	38.64	149.64	UTM	WGS84	45	30	North up 0.16
2	27/02/15	LANDSAT-8	OLI	139	44	49.03	137.39	UTM	WGS84	45	30	North up 1.72
3	15/03/15	LANDSAT-8	OLI	139	44	54.29	131.90	UTM	WGS84	45	30	North up 0.39
4	29/04/15	LANDSAT-8	OLI	139	44	66.76	107.89	UTM	WGS84	45	30	North up 0.00
5	02/05/15	LANDSAT-8	OLI	139	44	67.04	105.86	UTM	WGS84	45	30	North up 15.67
6	16/06/15	LANDSAT-8	OLI	139	44	68.32	84.70	UTM	WGS84	45	30	North up 14.68
7	10/07/15	LANDSAT-5	TM	139	44	64.70	86.48	UTM	WGS84	45	30	North up 34.00
8	19/08/15	LANDSAT-8	OLI	139	44	64.74	109.87	UTM	WGS84	45	30	North up 10.00
9	07/09/15	LANDSAT-8	OLI	139	44	62.16	123.84	UTM	WGS84	45	30	North up 0.08
10	25/10/15	LANDSAT-8	OLI	139	44	50.10	149.55	UTM	WGS84	45	30	North up 0.01
11	26/11/15	LANDSAT-8	OLI	139	44	41.84	154.42	UTM	WGS84	45	30	North up 0.02
12	28/12/15	LANDSAT-8	OLI	139	44	38.20	152.02	UTM	WGS84	45	30	North up 0.03

and physical properties of the sediment type, sensor observation angle, etc. (Ritchie and Schiebe 1986; Chen et al. 1991; Novo et al. 1991; Somvanshi et al. 2011). Thus NDTI technique plays a crucial role to identify and quantify the sediment character of reservoir and helps to achieve seasonal variation of different turbidity cover of the Panchet reservoir which is the desired goal of the present work. However, this band ratio technique has been applied for assessment of water turbidity of the Panchet Dam. In the present study, the NDTI image has been classified into high, medium and low turbidity zones on the basis of mean NDTI value and standard deviation computed by statistics of the images with the help of Arc GIS 10.2.1 version software. A comprehensive statistical measure is represented in Table 6 to know the maximum–minimum value, mean, standard deviation and range of NDTI values of different NDTI maps. The standard criterion or protocols to categorize the range of turbidity (low, medium and high) follows the formulae (Somvanshi et al. 2011):

$$\left. \begin{aligned}
 \text{Low Turbidity} &= \text{Mean} - \text{Standard Deviation} \\
 \text{Medium Turbidity} &= \text{Mean} + \text{Standard Deviation} \\
 \text{High Turbidity} &= \text{Value of more than Medium Turbidity}
 \end{aligned} \right\} (2)$$

Ranges of low, medium and high turbidity and their color in the standard false color composite (FCC) are represented in Table 7. Month-wise turbidity coverage maps of the Panchet reservoir are prepared on the basis of the above formulae.

Therefore, three qualitative turbidity ranges (low, medium and high) are followed for four different seasons of the Indian climate: Winter (January to March), Pre-monsoon (April to June), Monsoon (July to September) and Post-monsoon (October to December). The areal coverage of various types of NDTI ranges (high, medium and low) are calculated on the basis of unique pixel values derived from the NDTI maps prepared by the Arc GIS software version 10.2.1. Data, related with different turbidity classes (high, medium and low) of 2015 are presented in Table 8, which also shows the seasonally variation in turbidity of the Panchet Dam.

Relations among total suspended sediments (TSS), turbidity and NDTI

Sediments less than 2μ size is considered as dissolved sediment whereas larger than 2μ size found in water column is known as suspended sediment or floating sediment. Total suspended sediments (TSS) change physical look of water into cloudy, darkness or color and create opaque or muddy appearance that reduce water clarity. Turbidity of water is measured on the basis of amount of light scattered by particles in water column. More presence of particles, more scattering of light, thus turbidity and TSS is positively

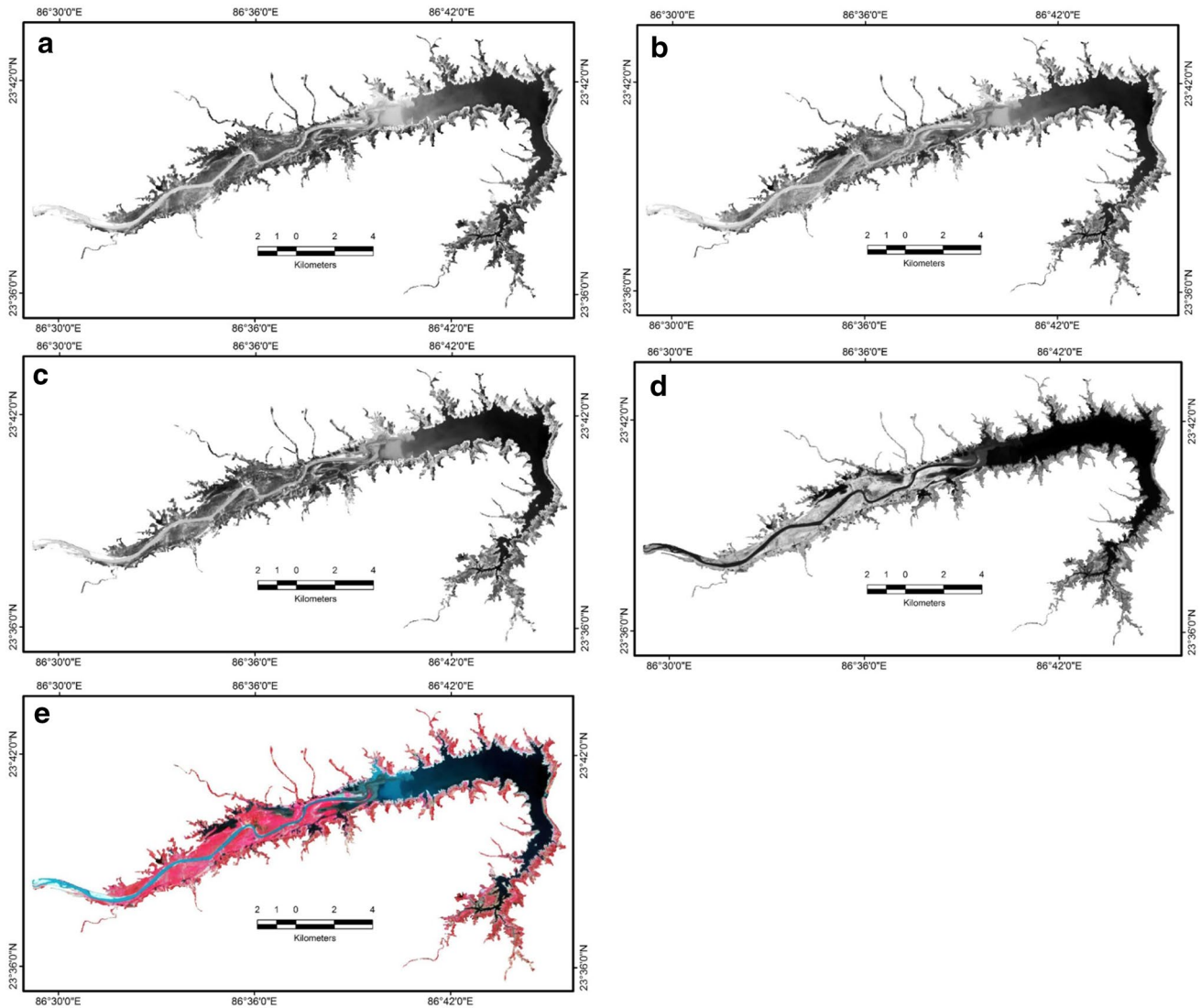


Fig. 6 Band reflectance from the reservoir water. **a** Reflectance in 2nd band (**b**). Reflectance in 3rd band (**c**). Reflectance in 4th band (**d**). Reflectance in 5th band (**e**). FCC combination

correlated to each other. More concentration of suspended sediment indicates more turbid character of water. Stream flow and turbidity is positively related because of sufficient run-off supplies more sediment from upper catchment and wherefrom water flow is strong enough that helps to increase turbidity by re-suspension of sediments settled on the bottom of the reservoir (Fondriest Environmental, Inc. 2014). Significant and positive relation has been established between turbidity and concentration of suspended sediment.

Total suspended sediments (TSS) is measured in the unit of mg/L. Turbidity meter is one of the most effective instruments to measure water turbidity and the result is reported in a unit which is known as Nephelometric Turbidity Unit (NTU). NTU is the standard unit of many broadband output (400–680 nm wavelengths) turbidity

meters. Total suspended sediments concentration lower than 20 mg/L appears clear in most situations whereas more than 40 mg/L levels starts to appear cloudy. In comparison, a turbidity reading below 5 NTU appears clear, while a reading of 55 NTU will start to look cloudy and a reading over 500 NTU will appear completely opaque (Fink 2005; EPA 2012; Chesapeake Bay Program 2012; Perlman 2014; Fondriest Environmental, Inc. 2014; Wood 2014). Positive relation has been established between NDTI values and TSS concentration directly which is analyzed in the discussion part of the present work and finally a strong positive relation is established between NDTI and turbidity ($p < 0.05$). Total suspended sediments (TSS) in mg/L and turbidity measured in turbidity units make a linear regression analysis and the relationship is shown

Fig. 7 Randomly selected 15 in situ stations for collection of water samples

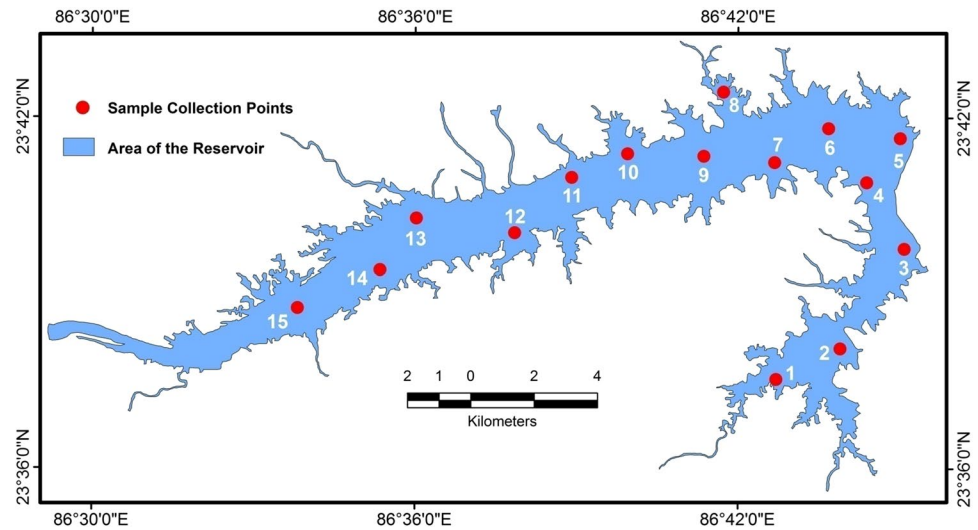


Table 6 Important NDTI values of individual month acquired from different processing steps of NDTI in Arc GIS software version10.3

Month	Count	Minimum	Maximum	Sum	Mean	SD	Range
January	80,670	−0.051719468	0.025458157	−2131.573155	−0.026423369	0.013491134	0.077177625
February	80,670	−0.058291566	0.026870665	−2756.752537	−0.034173206	0.014804155	0.085162231
March	80,670	−0.080103636	0.055534851	−2815.910013	−0.034906533	0.025834137	0.135638487
April	80,670	−0.070128582	0.060111448	−3006.746134	−0.037272172	0.023732742	0.130240030
May	80,670	−0.071867831	0.048679043	−3157.489696	−0.039140783	0.014012382	0.120546874
June	80,670	−0.082890294	0.050325811	−3036.794971	0.037644663	0.020291835	0.133216105
July	80,670	−0.121951222	0.151515156	−764.6325115	−0.009478524	0.040193018	0.273466378
August	80,670	−0.102110788	0.057588343	−2172.843079	−0.026934958	0.029811938	0.159699131
September	80,670	−1.000000000	0.046031445	−3883.535456	−0.048295472	0.014625936	1.046031445
October	80,670	−0.092028983	0.062528700	−3103.682308	−0.038473811	0.019292607	0.154557683
November	80,670	−0.056599371	0.025443403	−2509.621638	−0.031109727	0.01330667	0.082042774
December	80,670	−0.047420826	0.084261037	−2380.454719	−0.02950855	0.011061736	0.131681863

Table 7 Principle of different turbidity range and hue on FCC

Range of turbidity	Formula	Hue on false color composite (FCC)
Low	Mean − standard deviation (SD)	Dark blue to blackish
Medium	Mean + standard deviation (SD)	Medium blue
High	> Medium	Light blue to whitish blue

with the following equation (Fink 2005; Bin Omar and Bin MatJafri 2009):

$$NTU = a * (TSS)^b, \tag{3}$$

where NTU = turbidity measurement, TSS = total suspended sediments in mg/L, *a* = regression-estimated coefficient, *b* = regression-estimated coefficient.

Reading of EPA 180.1 turbidity meter in NTU unit and ISO 7027 turbidity sensor in FNU (formazin nephelometric units) unit are often similar (Fondriest Environmental, Inc. 2014).

Turbidity-based NDTI helps to develop a crucial mathematical identity to quantify siltation in reservoir and dams on the basis of linear regression model represented by Eq. 4 (Fondriest Environmental, Inc. 2014):

$$\text{Log}_{10}(\text{TSS}) = a * \text{Log}_{10}(\text{Turb}) + b, \tag{4}$$

where TSS = total suspended sediments in mg/L, Turb = turbidity in formazin nephelometric units (FNU), *a* = regression coefficient, *b* = Duan’s bias correction factor.

Table 8 Turbidity ranges and seasonal variation in 2015 calculated on the basis of NDTI formula using Arc GIS software of 10.3 version

Season	Month	Range of turbidity		
		Low	Medium	High
Winter	January	−0.039914503	−0.012932235	> −0.012932235
	February	−0.048977361	−0.019369051	> −0.019369051
	March	−0.060740670	−0.009072396	> −0.009072396
Pre-monsoon	April	−0.061004914	−0.013539430	> −0.013539430
	May	−0.053153165	−0.025128401	> −0.025128401
	June	0.017352828	0.057936498	> −0.057936498
Monsoon	July	−0.049671542	0.030714494	> 0.030714494
	August	−0.056746896	0.002876980	> 0.002876980
	September	−0.062921408	−0.033669536	> −0.033669536
Post-monsoon	October	−0.057766418	−0.019181204	> −0.019181204
	November	−0.044416397	−0.017803057	> −0.017803057
	December	−0.040570286	−0.018446814	> −0.018446814

Results and discussion

Seasonal distribution of turbid water

Winter, pre-monsoon, monsoon and post-monsoon are the four broad seasons of the Indian monsoon climate. 12 turbidity maps of the year 2015 are grouped into the above four seasons to interpret and analyze the seasonal variation of turbidity of the Panchet Hill Dam water. Each map shows three different turbidity zones, viz. low, medium and high over the 27.92 km² area of the reservoir. In the winter season (Fig. 8a), low turbid water exists in the inner part of the dam due to stagnation of water and it shares maximum area rather than other categories. Medium turbid zone is observed in between the low and high turbid zone, but maximum incidence of high turbid water is in the periphery of the dam. Though the amount of runoff is very low in this season, the peripheral area of the dam is supplied more sediment by the local small streams. In the pre-monsoon period (Fig. 8b), due to absence of rainfall, almost the whole area of the dam is covered by low turbid water except the entry part of the main river Damodar and some fringe areas of the dam. The picture is completely reversed in the monsoon period (Fig. 8c). Due to torrential rainfall and excess runoff, ample size of sediment is supplied to the dam from the upper catchment area dominated by sedimentary rock which is easily erodible in nature. More than 50% area is covered by highly turbid water and almost 80% area remains under medium and high turbid water in monsoon season. August is the peak monsoon month and delivers vast amount of dissolved sediment that results high turbidity. The post-monsoon season (Fig. 8d) is characterized by the less amounts of rainfall and runoff, so water turbidity remains medium to low. Only the parts confluenting the stream with the reservoir shows high turbid area. A superimposed view over seasonal changes of

high, medium and low categories of turbidity coverage in 2015 is presented in Fig. 9.

Variation of different types of turbidity

Different types of turbidity (high, medium and low) vary throughout the year for the Panchet Hill Dam water. Variation of turbidity is clearly analyzed with Fig. 10 and interpreted under the followings heads.

Variation in high turbidity

The high turbidity in winter season covers 4.37 km², 1.87 km² and 5.2 km² area in the months of January, February and March, respectively. The fact is almost same for the pre-monsoon season where the area coverage is 3.05 km², 3.75 km² and 4.13 km² in the months of April, May and June correspondingly, but the result is completely reversed in the monsoon period. Sufficient supply of runoff and dissolved sediment with it leads to more and more turbidity in water. Surface runoff of the area is highly turbid in the monsoon period because of domination of dissolved sediment as the upper catchment of the dam covered by erodible sedimentary rock. Owing to the adequate supply of surface runoff, a flash of flowing water strikes on the sediment already deposited in the reservoir and increases the water turbidity by the process of re-suspension of the sediment settled at the bottom of the reservoir (Somvanshi et al. 2011). July, August and September months cover 14.12 km², 17.3 km² and 14.74 km² area, respectively, under high turbidity of the reservoir. The situation repeats to its previous form in the post-monsoon season. The areal coverage under the high turbidity is 3.69 km², 5.75 km² and 7.07 km² in the last three months of the year, viz. October, November and December correspondingly.

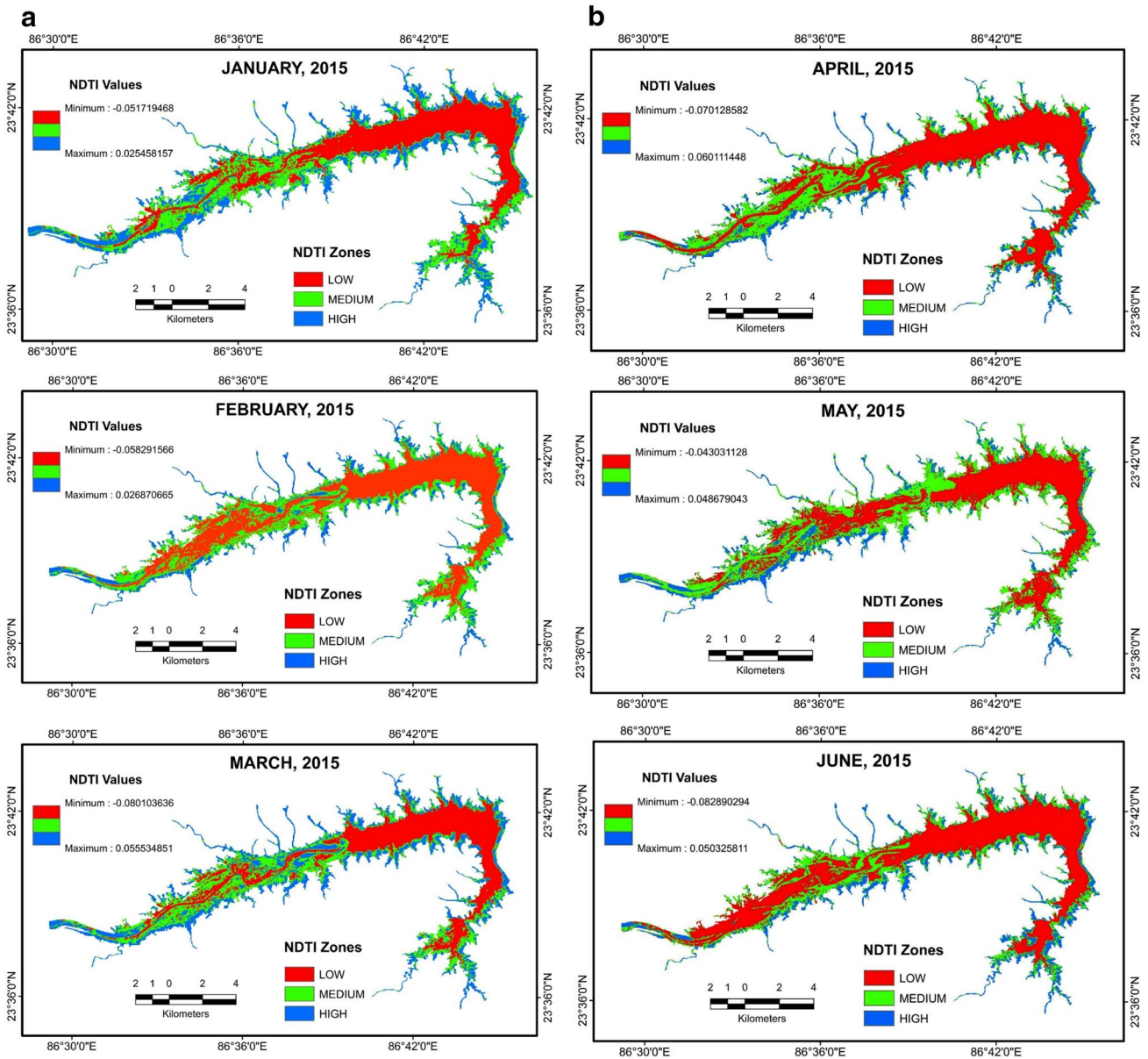


Fig. 8 Variation of water turbidity in **a** winter season, **b** pre-monsoon period, **c** monsoon period and **d** post-monsoon period

Variation in medium turbidity

The variation of medium turbidity seems insignificant from January to August as it remains almost same. The areas under that type of turbidity cover 6.83 km², 4.94 km², 6.85 km², 5.82 km², 7.54 km², 4.14 km², 8.52 km² and 4.78 km², respectively, from January to August. Only September and October months exceed the coverage of 10 km² of the particular type of turbidity. Figure 10c, d highlights that the areal coverage in September is 11.14 km², whereas October shares maximum coverage of 12.26 km² and proves into the inter-seasonal variation of medium turbidity cover in the Panchet reservoir.

Variation in low turbidity

More than 50% dam area covered by low turbid water in winter and pre-monsoon seasons. The coverage area in the months of January, February and March are 16.72 km², 21.11 km² and 15.87 km² correspondingly. Similarly, April, May and June cover 19.05 km², 16.63 km² and 21.65 km² area of low turbidity. The picture of monsoon season is just opposite to the winter and pre-monsoon. July, August and September cover a little share of low turbidity over the total area and the values are 5.28 km², 5.21 km² and 2.04 km² in that order. The post-monsoon season also covers more than 10 km² area of low turbidity and the quantity of the coverage

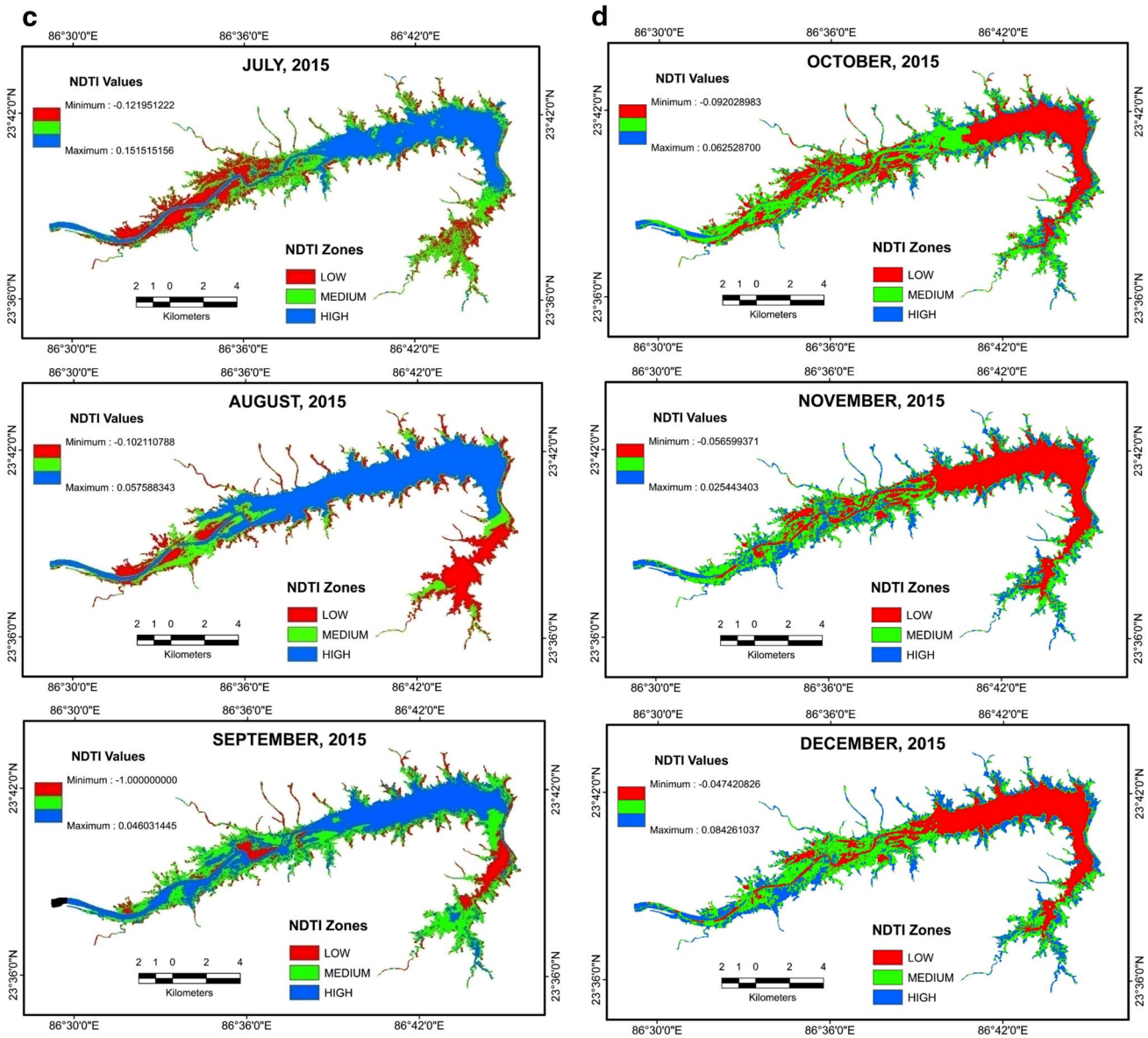


Fig. 8 (continued)

is 11.97 km², 13.65 km² and 12.40 km² in the months of October, November and December, respectively. Various statistical measures related with of the variation studies are included in Table 9 and on the basis of this statistics a box plot and whisker plot diagram have been drawn (Fig. 11) that prove into the significance of seasonal variation ($p < 0.05$) of water turbidity in the Panchet Hill Dam.

Seasonal variation of water turbidity

The Panchet reservoir has experienced a significant seasonal variation of water turbidity. In the winter season, maximum and minimum values of NDTI are -0.057 and 0.021 , respectively, while it varies from -0.039 to 0.043 in

the pre-monsoon period, -0.050 to 0.052 in the monsoon period and -0.052 to 0.021 in the post-monsoon period. A box plot and whisker plot diagram based on mean (\bar{X}) and standard deviation (SD) of NDTI result are shown in Fig. 12a to analyze the significance of variation ($N = 15$, $p < 0.05$) of water turbidity in different seasons. Winter and post-monsoon periods have negative mean value of NDTI and standard deviations are 0.030 and 0.026 , respectively, whereas pre-monsoon and monsoon periods have positive mean NDTI value with 0.029 and 0.026 standard deviation correspondingly. The mentioned statistical parameters (\bar{X} and SD) clearly indicate a significant inter-seasonal variation of NDTI in the Panchet Dam. Figure 12b represents variation in total suspended sediments (TSS) concentration

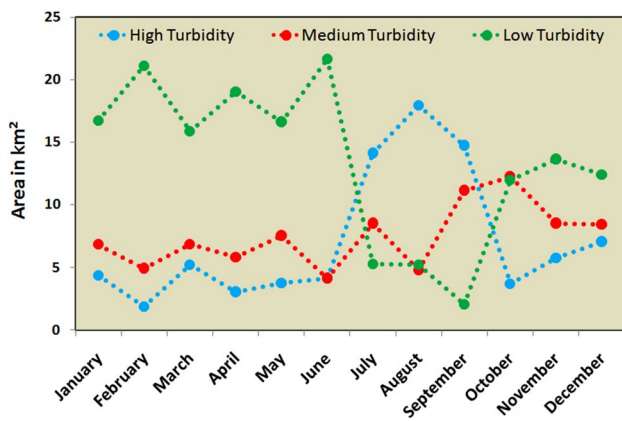


Fig. 9 Superimposition of high turbidity, medium turbidity and low turbidity coverage of the Panchet Dam, 2015

in mg/L of four different seasons and indirectly indicates a robust significance of inter-seasonal variation of water turbidity ($N = 15, p < 0.05$). Average TSS concentration is 59.07 mg/L, 88.07 mg/L, 106.6 mg/L and 49.47 mg/L in the period of winter, pre-monsoon, monsoon and post-monsoon seasons, respectively. In the winter season, maximum TSS concentration is found near sample point 15 (132 mg/L) and

minimum is near point number 4 (17 mg/L). The amount of highest and lowest TSS concentration in the pre-monsoon period is 156 mg/L (near point 10) and 13 mg/L (near point 6). TSS amount is quite high in this period compared to the winter season. It jumps into 182 mg/L (near point 12) in the monsoon period due to supply of sufficient sediment with surface runoff. In the post-monsoon period, maximum and minimum TSS concentration is 102 mg/L (near point 13) and 8 mg/L (near point 6), respectively. Average TSS concentration is 59.07 mg/L, 88.07 mg/L, 106.6 mg/L and 49.47 mg/L in the winter, pre-monsoon, monsoon and post-monsoon period correspondingly. Standard deviation of TSS concentration in the pre-monsoon and monsoon period is more than 50 which is quite high (pre-monsoon 51.46, monsoon 53.09) than winter and post-monsoon period (winter 39.67, post-monsoon 30.76). The statistical analysis clearly explains a significant inter-seasonal variation of water turbidity in the Panchet Dam throughout the year.

Relationship among different types of turbidity

Figure 13 shows the relationship among the three types of turbidity: high, medium and low. The trend line set in Fig. 13a reveals that the relationship between the area

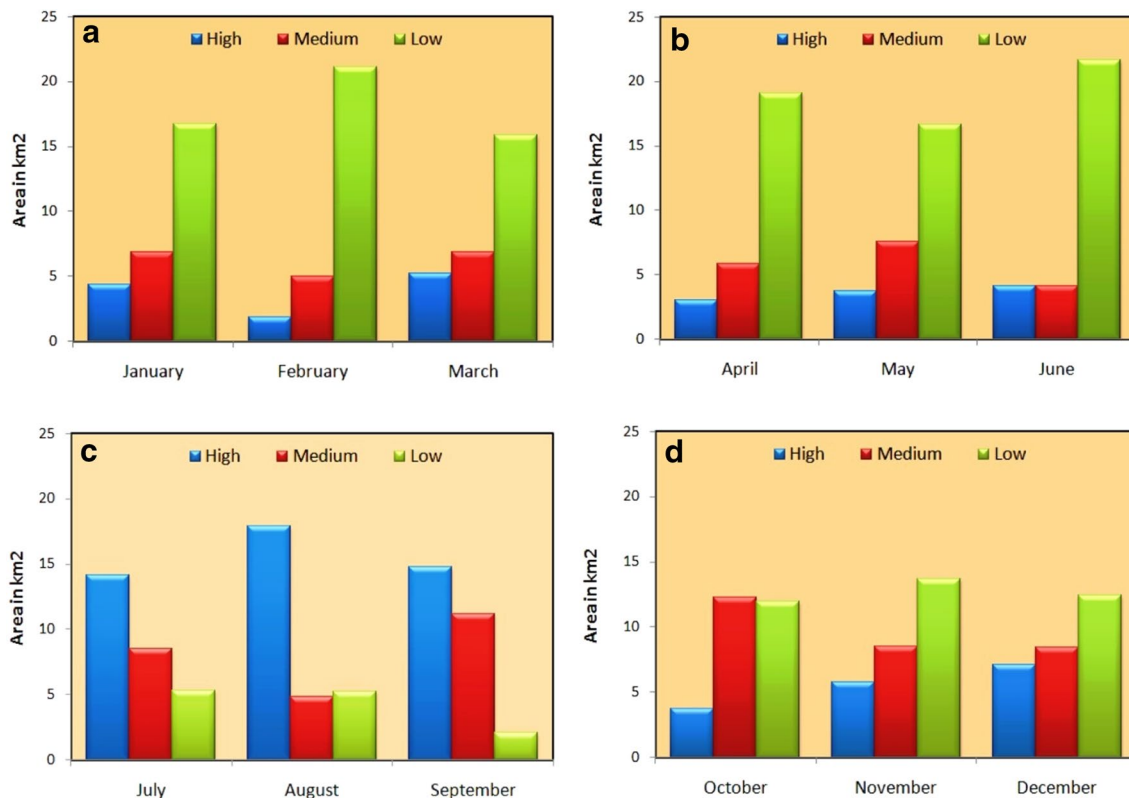
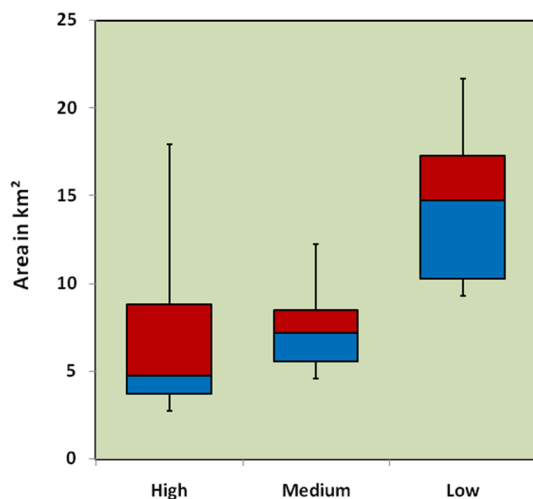


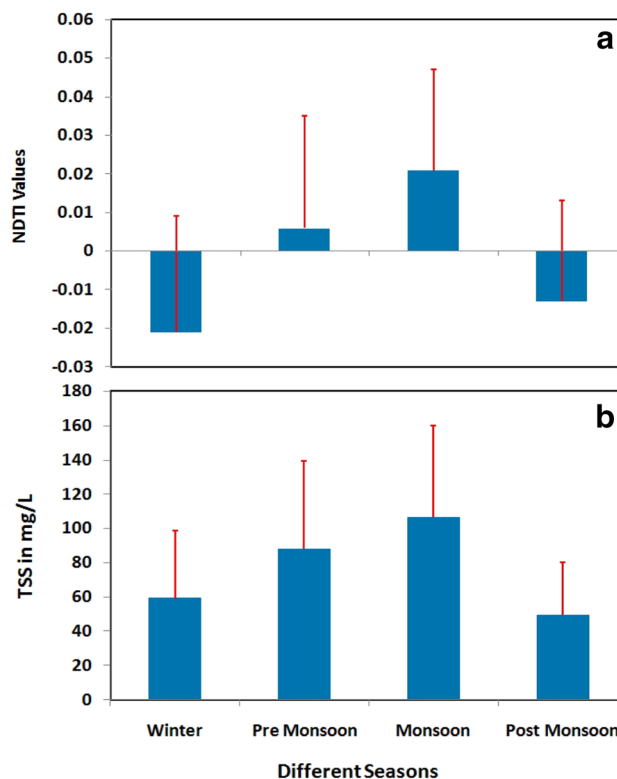
Fig. 10 Seasonal variation in areal coverage of different turbidity zone. **a** Winter season, **b** pre-monsoon period, **c** monsoon period, **d** post-monsoon period

Table 9 Statistical measures of different turbidity coverage

Categories	Statistical parameters of the turbidity coverage (km ²)										
	Minimum	Maximum	Average	Range	Q1	Median	Q3	Inter quartile range	Skewness	Kurtosis	SD
High	1.87	17.93	7.14	16.06	3.74	4.79	8.83	5.09	1.21	−0.0002	5.34
Medium	4.14	12.26	7.48	8.12	5.60	7.20	8.52	2.92	0.59	−0.1743	2.48
Low	2.04	21.65	13.47	19.61	10.30	14.76	17.30	7.00	−0.56	−0.7404	6.41

**Fig. 11** Box plot and whisker plot diagram (based on quartile deviation) showing the variation of high, medium and low types of turbidity coverage, 2015 ($p < \alpha$, $p < 0.05$)

of high and medium turbidity is positive but the degree of strength is very low because of their poor association ($R^2 = 0.020$). The relation is statistically significant at the significance level of 0.05% ($p < 0.05$). The trend illustrates that the months which have more coverage of high turbidity area have less relation with the coverage of medium turbidity area. This relation clearly indicates the area of medium turbidity that remains same with the area of high turbidity. There is no considerable change in medium turbidity area instead of increase in high turbidity area. Figure 13b displays very strong negative relationship between high turbidity area and low turbidity area ($R^2 = -0.817$). The relation is statistically significant at the significance level of 0.01% ($p < 0.01$). The trend line exemplifies that high turbidity area has an increasing change with the decreasing trend of low turbidity area and reveals amount of low turbidity area has been significantly decreased. A vice versa relation has been established between these types of turbidity. Months dominated by high turbidity area experience least amount of low turbidity area and which have been dominated by low turbidity area that has experienced minimal coverage of high turbidity. Scatter diagram and trend line shown in Fig. 13c explains

**Fig. 12** Box plot and whisker plot based on mean and standard deviation show significant seasonal variation ($p < 0.05$) of turbidity. **a** Variation in NDTI-based turbidity. NDTI values are derived from the prepared maps **(b)**. Variation in measured turbidity. TSS data (mg/L) is collected through field survey and laboratory analysis

the relationship between medium turbidity area and low turbidity area. These two parameters have established a poor negative relationship ($R^2 = -0.297$) and is statistically significant at the level of 0.05% level of significance ($p < 0.05$). Area of medium turbidity has been increased with the decrease of low turbidity area and low turbidity area has been increased with the decreasing trend of medium turbidity area. These relationships scientifically explain that a strong significance has been experienced on variation of water turbidity by the Panchet Dam throughout the year and more specifically during different seasons. In the monsoon period area of high turbidity is greater while low turbidity cover has a smaller amount. On opposite side

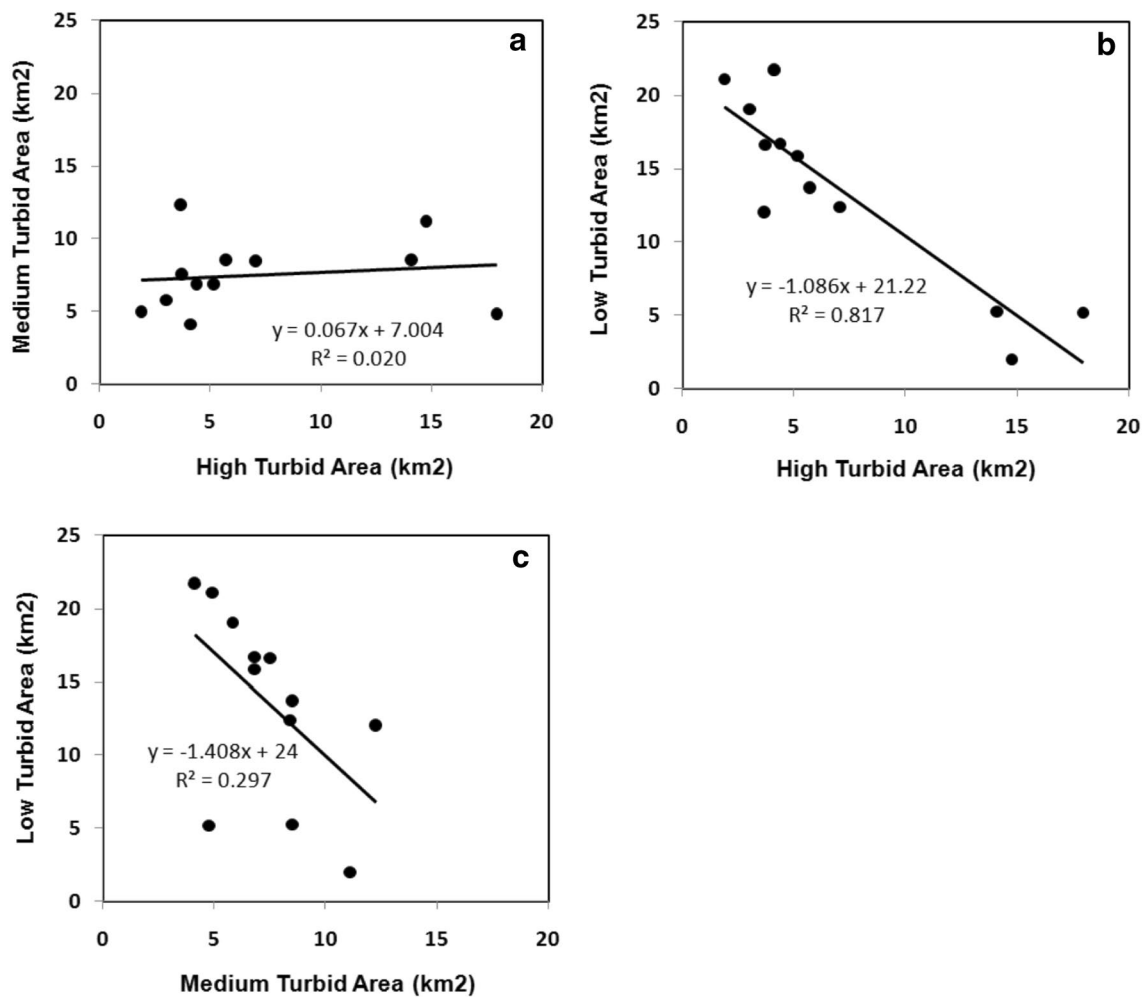


Fig. 13 Relation among different types of turbidity: **a** relationship between high and medium turbidity coverage ($p < 0.05$), **b** relationship between high and low turbidity coverage ($p < 0.01$), **c** relationship between medium and low turbidity coverage ($p < 0.05$)

in the winter and pre-monsoon period maximum area of the reservoir is covered by low turbidity area while amount of high turbidity area is minimal. Medium turbidity area remains high only in the post-monsoon period but high turbidity area is very less in this time.

Relation of NDTI with measured turbidity

Theoretically NDTI and turbidity are positively correlated and it has been discussed in previous section of the work. Now we analyze how these relations of the parameters vary in different seasons in the Panchet Dam. Turbidity is represented by TSS concentration in mg/L. More than 40 mg/L concentration of sediments appears to be of turbid nature (Fink 2005; EPA 2012; Chesapeake Bay Program 2012; Perlman 2014; Fondriest Environmental, Inc. 2014; Wood 2014). Figure 14a–d represents relationships between NDTI and TSS concentration of the Panchet Dam in the winter, pre-monsoon, monsoon and post-monsoon

periods, respectively. In winter period NDTI and turbidity level is highly correlated in terms of positive relation and significant in 0.05% level of significance ($p < 0.05$) with minimal standard error ($R^2 = 0.926$, SEE/RMSE = 10.39). Maximum NDTI value is less than 0.03 and TSS concentration is less than 140 mg/L in this period. Degree of association is quite less in the pre-monsoon period than winter ($R^2 = 0.866$, SEE/RMSE = 18.14, $p < 0.05$) and maximum value of NDTI and TSS concentration are 0.043 and 156 mg/L, respectively. In the monsoon period, both NDTI and TSS concentration are relatively high than other seasons. Maximum NDTI values exceed 0.05 and TSS concentration is more than 180 mg/L in monsoon period. A positive relation has been established between these parameters and standard error is relatively high ($R^2 = 0.847$, SEE/RMSE = 20.02, $p < 0.05$). Trend line fitted for the post-monsoon period shows high correlation between NDTI values and TSS concentration with minimum standard error ($R^2 = 0.961$, SEE/RMSE = 5.80,

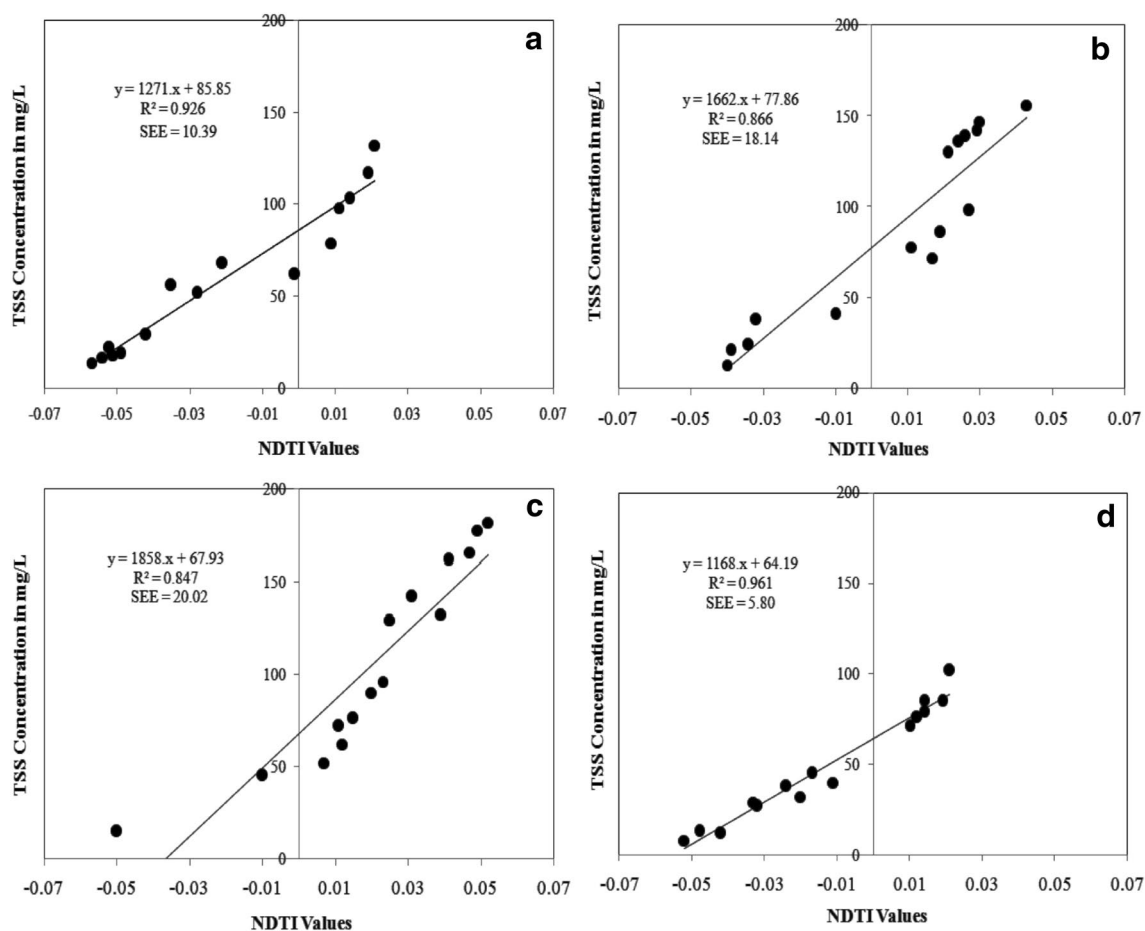


Fig. 14 Relation between measured turbidity (TSS in mg/L) and NDTI map-based turbidity (NDTI values) ($p < 0.05$). **a** Relation exists in winter season **(b)**. Relation exists in pre-monsoon period **(c)**. Relation exists in monsoon period **(d)**. Relation exists in post-monsoon period

$p < 0.05$). Maximum level of NDTI shows 0.021 while TSS concentration is 102 mg/L in this post-monsoon period.

The study investigates that in the periods of winter, pre-monsoon and post-monsoon, turbidity level of the dam ranged within 60 NTU, which indicates quite clear to slight cloudy appearance of water, but it easily jumps into 100–700 NTU in the monsoon period due to heavy rainfall and supply of ample sediments with surface runoff that represents high level of turbidity and almost opaque to completely opaque appearance of the water.

Accuracy assessment and validation of the work by field investigation

Accuracy assessment and validation of the research work is crucial for acceptance of the derived result. Accuracy assessment of the present work is performed on the basis of ground truth values collected through rigorous field survey. 15 samples are taken from each types of turbidity (high, medium and low) to compare the NDTI result and total sample converted into 45 ($N = 15 \times 3$). Accuracy

assessments of different types of turbidity are performed based on error matrix. User's accuracy, producer's accuracy, overall accuracy and Kappa coefficient are used to validate the result (Jensen 2015). User's accuracy level for high, medium and low turbidity is 86.67%, 80.00% and 86.67%, respectively, whereas producer's accuracy level is 81.25%, 75.00% and 100% for high, medium and low turbidity correspondingly. Overall accuracy and Kappa coefficient are 84.45% and 76.64% of the work, respectively, that indicate a reliable and trustworthy result to the audiences and promise a robust validation of the work. Error matrix and summary of accuracy assessments result for different types of turbidity is shown in Table 10. Average correlation coefficient value (R^2) between satellite derived turbidity (NDTI) and ground level turbidity of different seasons is 0.90 with 0.05% level of significance and root mean square error (RMSE) or standard error of estimate (SEE) value is 13.59. This strongly positive correlation and minimal SEE/RMSE further approve the validity of the result. Field investigation photos of different turbid water are shown in Fig. 15.

Table 10 Summary of accuracy assessment results for different types of turbidity

Error matrix for different types of turbidity					
Turbidity derived from ground truth values*					
	High	Medium	Low	Total	User's accuracy
<i>Turbidity derived from NDTI maps</i>					
High	13	2	0	15	86.67%
Medium	3	12	0	15	80.00%
Low	0	2	13	15	86.67%
Total	16	16	13	45	
Producer's accuracy	81.25%	75.00%	100%		
Overall accuracy:	84.45%				
Kappa coefficient:	76.64%				

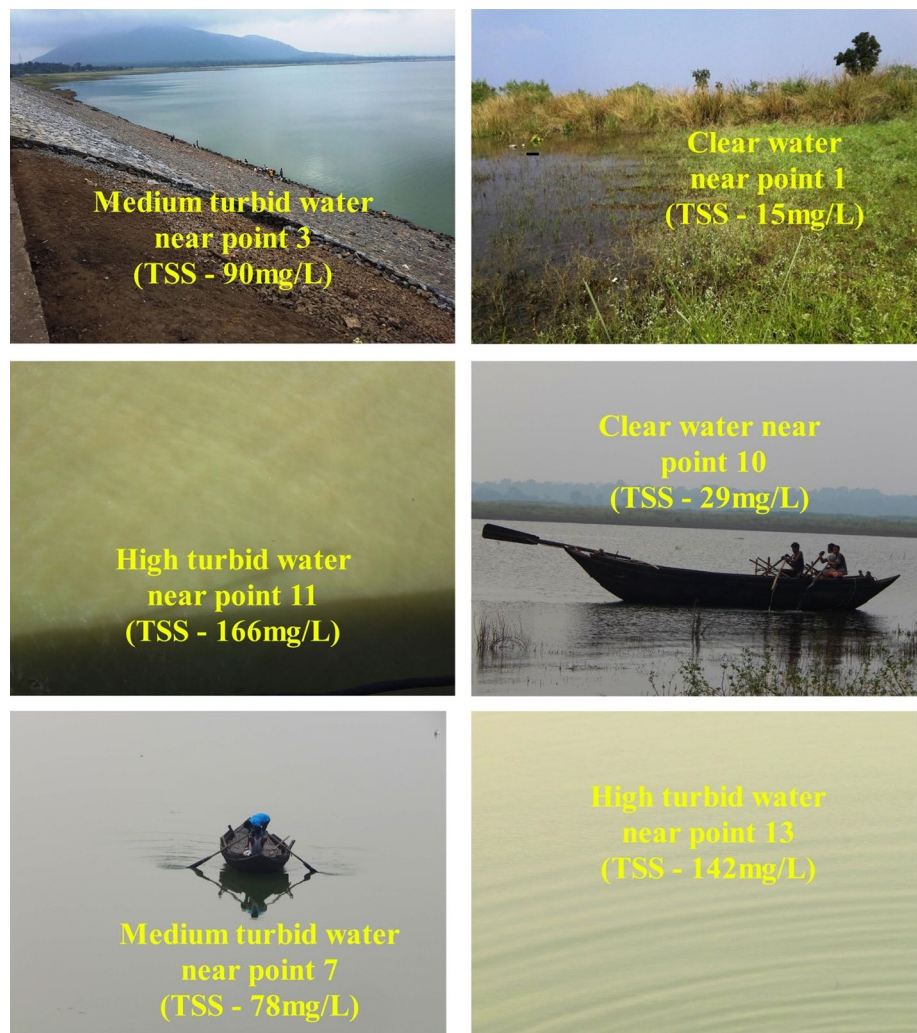
*Ground truth values are represented in terms of TSS concentration in mg/L. <40 mg/L—low turbidity, 40–100 mg/L—medium turbidity, >100 mg/L—high turbidity level is considered (Fondriest Environmental, Inc. 2014)

The most relevant factor of the approach used in the work is accuracy level of the NDTI technique. More than 80% overall accuracy level in ground truth verification is highlighted in the result of accuracy assessment. It is very effective approach for regular monitoring of dam sediment. A valid relationship among turbidity, TSS and NDTI is established. Many previous works related with sediment monitoring and management based on remote sensing provide only mapping part. This work quantifies the sediment load and area of different turbidity zones.

Conclusion

The entire work indicates a sophisticated use of remote sensing technique to monitor the water quality and sedimentation in a reservoir. It also helps to estimate the total suspended sediments (TSS) load of the reservoir. In the third world country like India it is impossible to frequent sponsor for the measurement and monitoring the different water parameters

Fig. 15 Field investigation photos of different turbid water



of the reservoir and this circumstances can be overcome using the easily available NDTI technique. This work has immense potentiality for quantifying any reservoir sediment volume and identifying the zones of different turbid areas that help for planning and sustainable management of reservoir sediment. Seasonal variation of water turbidity in the Panchet Dam is proven by the result of Box plot diagrams and parameterization graphs which is prime goal of the present study. Box plot diagram based on quartile deviation statistically explains that the dam has a significant seasonal variation of water turbidity ($p < \alpha$, $p < 0.05$) due to seasonal variation of total suspended sediments (TSS). The average seasonal correlation value (R^2) between NDTI values and TSS concentration is 0.90 and error of these parameters is 13.59 (RMSE) that again strongly recommends and legalizes the broad use of the technique in the field of hydrology, water monitoring and management. The result of this work indicates that due to excessive siltation the Panchet reservoir will be blocked within 200 years and many villages located in the upper catchment area will be inundated through upward spreading of dam water. Water is contaminated day by day through the deposited sediment. Nutrient elements are trapped in the reservoir through sediment deposition and it is exclusively responsible for eutrophication process. In the Panchet reservoir phosphorus is imported through the trapping of sediment particles known as important macronutrient and assists to grow algal bloom, phytoplankton or floating macrophytes that cover half of the reservoir's surface area. It reduces the supply of dissolved oxygen and damages live organism of the reservoir. Floating plants residual are decomposed and create methane that contaminates the water by unpleasant smell, color and test. Afforestation of indigenous species and soil conservation at the upper catchment area of the dam are the major recommendations to check the supply of the sediment to the reservoir. To maintain the water quality of the dam it is recommended for implementing sediment bypass system or flushing of sediment through spillway. Sediment trapping in the upper catchment area by building of check dams and dredging of sediment are the other recommendations for sediment management.

Though NDTI technique can obtain data from inaccessible areas without disturbing any object it has many flaws. In many cases, user compelled to use cloudy data that carries some error in result. Highly complex inland topography, especially in hilly area where water bodies have some shadow effects and vegetation cover, water reflectance bands are deviated from its actual reflectance. In the marine environment, due to wave effect acquisition of correct spectral reflectance of suspended sediment is absolutely not possible.

Acknowledgements The corresponding author wishes to acknowledge the University Grand Commission, New Delhi, India, for the financial support [JRF Award Letter No. F.15-6(DEC.2013)/2014(NET),

UGC-Ref. No.: 3154/(NET-DEC.2013)] to carry out this research work. The authors would like to thank two anonymous reviewers for their comments and suggestions to enrich the work.

References

- Aguirre-Gomez R (2000) Detection of total suspending sediments in the North Sea using Avhrr and ship data. *Int J Remote Sens* 21:1583–1596
- Alka S, Sushma P, Singh TS, Patel JG, Tanwar H (2014) Wetland information system using remote sensing and GIS in Himachal Pradesh, India. *Asian J Geoinform* 14(4):13–22
- Bhattacharya BK, Chakraborti BR, Sen NN, Mukherji S, Ray P, Sengupta S, Sengupta KS, Sen NN, Maity T (1985) West Bengal District Gazetteers. Puruliya, pp 2–22
- Bid S (2016) Change detection of vegetation cover by NDVI technique on catchment area of the Panchet Hill Dam, India. *Int J Res Geogr* 2(3):11–20, ISSN 2454-8685. <http://dx.doi.org/10.20431/24548685.0203002>
- Bin Omar AF, Bin MatJafri MZ (2009) Turbidimeter design and analysis: a review on optical fiber sensors for the measurement of water turbidity. In: *Sensors* (Basel). Retrieved from <http://www.ncbi.nlm.nih.gov/pmc/articles/PMC3292109/>
- Bonakdari H, Zaji AH, Binns AD, Gharabaghi B (2019) Integrated Markov chains and uncertainty analysis techniques to more accurately forecast floods using satellite signals. *J Hydrol* 572:75–95. <https://doi.org/10.1016/j.jhydrol.2019.02.027>
- Borland WM, Miller CR (1958) Distribution of sediment in large reservoir. *J Hydraul Div* 84(2):1587.1–1587.10
- Campbell JB (1996) *Introduction to remote sensing*, 4th ed. Guilford Publications, New York, ISBN 1-59385-319-X
- Chalov S, Bazilova V, Tarasov M (2017a) Modeling suspended sediment distribution in the Selenga River Delta using landsat data. *Proc IAHS* 375:19–22. <https://doi.org/10.5194/piahs-375-19-2017>
- Chalov S, Golosov V, Tsyplenkov A, Zakerinejad R, Marker M, Samokhin M (2017b) A toolbox for sediment budget research in small catchments. *Geogr Environ Sustain* 10(4):43–68. <https://doi.org/10.24057/2071-9388-2017-10-4-43-68>
- Chen Z, Hanson JD, Curran PJ (1991) The form of the relationship between suspended sediment concentration and spectral reflectance: its implication for the use of Daedalus 1268 data. *Int J Remote Sens* 12(1):215–222
- Chen CH, Fang L, Zhang L, Huang W (2009) Remote sensing of turbidity in seawater intrusion reaches of Pearl River Estuary—a case study in Modaomen water way, Estuarine, Coastal and Shelf Science
- Chesapeake Bay Program (2012) Water clarity. In: *The Bay Ecosystem*, Retrieved from <https://www.chesapeakebay.net/discover/bayecosystem/waterclarity>
- Collins AL, Walling DE (2004) Documenting catchment suspended sediment sources: problems, approaches and prospects. *Prog Phys Geogr* 28:159–196
- Doxaran D, Froidefond JM, Lavender S, Castaing P (2002) Spectral signature of highly turbid water application with SPOT data to quantify suspended particulate matter concentration. *Remote Sens Environ* 81(1):149–161
- EPA (2012) Turbidity. In: *Water: monitoring & assessment*. Retrieved from <http://water.epa.gov/type/rs/monitoring/vms55.cfm>
- Fink JC (2005) Chapter 4—establishing a relationship between sediment concentrations and turbidity. In: *The effects of urbanization on Baird creek, Green Bay, WI* (Thesis). Retrieved from http://www.uwgb.edu/watershed/fink/Fink_Thesis_Chap4.pdf

- Fondriest Environmental Inc. (2014) Turbidity, total suspended solids and water clarity, fundamentals of environmental measurements. <http://www.fondriest.com/environmental-measurements/parameters/water-quality/turbidity-total-suspended-solids-water-clarity>
- Gardelle J, Hiernaux P, Kergoat L, Grippa M (2010) Less rain, more water in ponds: a remote sensing study of the dynamics of surface waters from 1950 to present in pastoral Sahel (Gourma region, Mali). *Hydrol Earth Syst Sci* 14:309–324
- Garg V, Kumar AS, Aggarwal SP, Kumar V, Dhote PR, Thakur PK, Nikam BR, Sambare RS, Siddiqui A, Muduli PR, Rastogi G (2017) Spectral similarity approach for mapping turbidity of an inland waterbody. *J Hydrol* 550:527–537
- Geological Survey of India (1991) Government of India
- Ghosh S, Islam A (2016) Quaternary alluvial stratigraphy and Palaeoclimatic reconstruction in the Damodar River Basin of West Bengal. In: Das BC et al (eds) *Neo-thinking on Ganges Brahmaputra basin geomorphology*. Springer, Switzerland, pp 1–18. https://link.springer.com/chapter/10.1007/978-3-319-26443-1_1
- Grade RJ (2006) *River morphology*. New Age International Ltd, New Delhi
- Guchhait SK, Islam A, Ghosh S, Das BC, Maji NK (2016) Role of hydrological regime. In: *Channel and floodplain sediments in channel instability of Meandering Bhagirathi River, Ganga—Brahmaputra Delta, India, Physical Geography*. Taylor & Francis, USA. <https://www.tandfonline.com/doi/abs/10.1080/02723646.2016.1230986>
- Guyot G (1989) Signatures spectrales des surfaces naturelles. *Télétection satellitaire*, 5, Col. SAT, Ed. Paradigme, 178
- He GK, Shao MH, Gao BS, Liu RY (1994) The variable relations between the turbidity and suspended matter in the sea water during the dredging process of the channel in Dayao Bay. *Mar Environ Sci* 13:76–82 (in Chinese with English Abstract)
- Islam M, Sado K (2006) Analyses of ASTER and Spectroradiometer data with in situ measurements for turbidity and transparency study of lake Abashri. *Int J Geoinf* 2:31–45
- Issa IE, Ansari NA, Sherwany G, Knutsson S (2017) Evaluation and modification of some empirical and semi-empirical approaches for prediction of area-storage capacity curves in reservoirs of dams. *Int J Sedim Res* 32:127–135
- Jain SK, Singh VP (2003) *Water resources systems planning and management*. Elsevier, Amsterdam
- Jensen JR (2015) *Introductory digital image processing: a remote sensing perspective*. Prentice Hall, Upper Saddle River, NJ
- Kaveh K, Hosseinzadeh H, Hosseini K (2013) A new equation for calculation of reservoir's area-capacity curves. *KSCE J Civ Eng* 17(5):1149–1156. <https://doi.org/10.1007/s12205-013-0230-3>
- Kratzer S, Bowers D, Tett PB (2000) Seasonal changes in colour ratios and optically active constituents in the optical case-2 waters of the Menai Strait, North Wales. *Int J Remote Sens* 21:2225–2246
- Lacaux JP, Tourre YM, Vignolles C, Ndione JA, Lafaye M (2007) Classification of ponds from high-spatial resolution remote sensing: application to Rift Valley Fever epidemics in Senegal. *Remote Sens Environ* 106:66–74
- Mano V, Némery J, Belleudy P, Poirel A (2009) Assessment of suspended sediment transport in four alpine watersheds (France): influence of the climatic regime. *Hydrol Process*. <https://doi.org/10.1002/hyp.7178>
- Martínez-Carreras N, Udelhoven T, Krein A, Gallart F, Iffly JF, Ziebel J, Hoffmann L, Pfister L, Walling DE (2010) The use of sediment colour measured by diffuse reflectance spectrometry to determine sediment sources: application to the Atert River catchment (Luxembourg). *J Hydrol* 382:49–63
- Meybeck M, Laroche L, Dürr HH, Syvitski JP (2003) Global variability of daily total suspended solids and their fluxes. *Glob Planet Changes* 39:65–93
- Moeeni H, Bonakdari H (2017) Forecasting monthly inflow with extreme seasonal variation using the hybrid SARIMA-ANN model. *Stoch Environ Res Risk Assess* 31(8):1997–2010. <https://doi.org/10.1007/s00477-016-1273-z>
- Moeeni H, Bonakdari H, Ebtehaj I (2017) Integrated SARIMA with neuro-fuzzy systems and neural networks for monthly inflow prediction. *Water Resour Manag* 31(7):2141–2156. <https://doi.org/10.1007/s11269-017-1632-7>
- Mohammadzadeh-Habili J, Heidarpour M (2010) New empirical method for prediction of sediment distribution in reservoirs. *J Hydrol Eng* 15(10):813–821. [https://doi.org/10.1061/\(ASCE\)HE.1943-5584.0000259](https://doi.org/10.1061/(ASCE)HE.1943-5584.0000259)
- Mohammadzadeh-Habili J, Heidarpour M, Mousavi SF, Haghiabi AH (2009) Derivation of reservoir's area-capacity equations. *J Hydrol Eng* 9:1017–1023. [https://doi.org/10.1061/\(ASCE\)HE.1943-5584.0000074](https://doi.org/10.1061/(ASCE)HE.1943-5584.0000074)
- Molo VD, Piccazzo M, Ramella A, Giusto DD, Vernazza G (1989) Monitoring of coastal water quality through integration between 'in situ' measurements and remote sensing data. In: Hallikainen M (ed) *Proceedings of the ninth EARSeL symposium*, Espoo, 27 June–1 July 1989. Luxembourg: commission of the European Communities, Directorate General for Science Research and Development, pp 86–91
- Morris GL, Fan J (1998) *Reservoir sedimentation handbook, design and management of dams, reservoirs and watersheds for sustainable use*. McGraw-Hill, New York
- Novo EMM, Steffen CA, Braga ZE (1991) Results of a laboratory experiment relating spectral reflectance to total suspended solids. *Remote Sens Environ* 36:67–72
- Olmanson LG, Brezonik PL, Bauer ME (2013) Airborne hyperspectral remote sensing to assess spatial distribution of water quality characteristics in large rivers: the Mississippi River and its tributaries in Minnesota. *Remote Sens Environ* 130:254–256
- Papoutsas C, Retalis A, Toullos L, Hadjimitsis DG (2014) Defining the landsat Tm/Etm+ and Chris/Proba spectral regions in which turbidity can be retrieved in inland waterbodies using field spectroscopy. *Int J Remote Sens* 35:1674–1692
- Perlman H (2014) *Turbidity, the USGS Water Science School*. Retrieved from <http://water.usgs.gov/edu/turbidity.html>
- Qu Y, Qi H, Ayhan B, Kwan C, Kidd R (2017) Does multispectral/hyperspectral pansharpening improve the performance of anomaly detection? In: *IEEE international geoscience and remote sensing symposium (IGARSS)*
- Rahaman KR, Hassan QK, Ahmed MR (2017) Pan-sharpening of Landsat-8 images and its application in calculating vegetation greenness and canopy water contents. *Int J Geo-Inf* 6(168):1–15. <https://doi.org/10.3390/ijgi6060168>
- Ritchie JC, Schiebe FR (1986) Monitoring suspended sediments with remote sensing techniques. In: *Hydrologic application of space technology*, (Proceedings of the Cocoa Beach Workshop, FL, August 1985), pp 233–242. IAHS Pubf. No. 160
- Shaharum NSN, Shafri HZM, Gambo J, Abidin FAZ (2018) Mapping of Krau Wildlife Reserve (KWR) protected area using Landsat 8 and supervised classification algorithms. *Remote Sens Appl Soc Environ*. <https://doi.org/10.1016/j.rsase.2018.01.002>
- Sharma A, Panigrahy S, Singh TS, Patel JG, Tanwar H (2014) Wetland information system using remote sensing and GIS in Himachal Pradesh, India. *Asian J Geoinform* 14(4):13–22
- Siddique G, Bid S (2017) Ecological impact of the Panchet Dam: a review. *Res World J Arts Sci Commer* VIII(1(1)):104–112, ISSN 2231-4172
- Singh S, Banerji P (eds) (2002) *Large dams in India: environmental, social and economic impacts*. Indian Institute of Public Administration, New Delhi
- Somvanshi S, Kunwar P, Singh NB, Kachhwaha TS (2011) Water turbidity assessment in part of Gomti River using high resolution

- Google Earth's Quickbird satellite data. Geospatial World Forum, Hyderabad
- Spate OHK, Farmer BH (1954) *India and Pakistan—a regional geography*. Methuen & Co., Ltd., London
- Teodoro AC, Veloso-Gomes F, Goncalves H (2008) Statistical techniques for correlating total suspended matter concentration with seawater reflectance using multispectral satellite data. *J Coast Res* 24:40–49
- Townshend JR, Justice CO (1986) Analysis of dynamics of African vegetation using the normalised difference vegetation index. *Int J Remote Sens* 7:1435–1445
- Trinh LH, Zablotskii RV, Le TH, Dinh TTH, Le TT, Trinh TT, Nguyen TTN (2018) Estimation of suspended sediment concentration using VNREDSat—1A multispectral data, a case study in Red River, Hanoi, Vietnam. *Geogr Environ Sustain* 11(3):49–60. <https://doi.org/10.24057/2071-9388-2018-11-3-49-60>
- Tucker CJ, Sellers PJ (1986) Satellite remote sensing of primary productivity. *Int J Remote Sens* 7:1395–1416
- Tyler AN, Svab E, Presing M, Kovacs WA (2006) Remote sensing of the water quality of shallow lakes: a mixture modeling approach to quantifying phytoplankton in water characterized by high-suspended sediment. *Int J Remote Sens* 27:1521–1537
- Valdiya KS (2016) *The making of India—geodynamic evolution*, 2nd edn. Springer, Switzerland, p 418, ISBN 978-3-319-25029-8 (eBook)
- Verbyla DL (1995) *Satellite remote sensing of natural resources*. Lewis Publishers/CRC Press LLC, Boca Raton, p 224
- Wood MS (2014) Estimating suspended sediment in rivers using acoustic Doppler meters. In: U.S. Geological Survey Fact Sheet 2014-3038. N.p.: U S Geological Survey
- Zaji AH, Bonakdari H, Gharabaghi B (2018) Reservoir water level forecasting using group method of data handling. *Acta Geophys* 66(4):717–730. <https://doi.org/10.1007/s11600-018-0168-4>
- Zaji AH, Bonakdari H, Gharabaghi B (2019) Applying upstream satellite signals and a two-dimensional error minimization algorithm to advance early warning and management of flood water levels and river discharge. *IEEE Trans Geosci Remote Sens* 57(2):902–910. <https://doi.org/10.1109/TGRS.2018.2862640>

Publisher's Note Springer Nature remains neutral with regard to jurisdictional claims in published maps and institutional affiliations.